2007-11-28

Synthesis of Optimal Arrays For MIMO and Diversity Systems

Britton T. Quist
Brigham Young University - Provo

SYNTHESIS OF OPTIMAL ARRAYS FOR MIMO AND DIVERSITY SYSTEMS

by

Britton T. Quist

A thesis submitted to the faculty of

Brigham Young University

in partial fulfillment of the requirements for the degree of

Master of Science

Department of Electrical and Computer Engineering

Brigham Young University

December 2006

BRIGHAM YOUNG UNIVERSITY

GRADUATE COMMITTEE APPROVAL

of a thesis submitted by

Britton T. Quist

This thesis has been read by each member of the following graduate committee and by majority vote has been found to be satisfactory.

Date	Michael A. Jensen, Chair
Date	Karl F. Warnick
Date	Brian D. Jeffs

BRIGHAM YOUNG UNIVERSITY

As chair of the candidate's graduate committee, I have read the thesis of Britton T. Quist in its final form and have found that (1) its format, citations, and bibliographical style are consistent and acceptable and fulfill university and department style requirements; (2) its illustrative materials including figures, tables, and charts are in place; and (3) the final manuscript is satisfactory to the graduate committee and is ready for submission to the university library.

Date

Michael A. Jensen
Chair, Graduate Committee

Accepted for the Department

Michael J. Wirthlin
Graduate Coordinator

Accepted for the College

Alan R. Parkinson
Dean, Ira A. Fulton College of
Engineering and Technology

ABSTRACT

SYNTHESIS OF OPTIMAL ARRAYS FOR

MIMO AND DIVERSITY SYSTEMS

Britton T. Quist

Department of Electrical and Computer Engineering

Master of Science

This thesis proposes a method for determining the optimal antenna element radiation characteristics which maximize diversity gain given a specific power angular spectrum of the propagation environment. The method numerically constructs the eigenfunctions of the covariance operator for the scenario subject to constraints on the power radiated by each antenna as well as the level of supergain allowed in the solution. The optimal antenna characteristics are produced in terms of radiating current distributions along with their resulting radiation patterns. The results reveal that the optimal antennas can provide significantly more diversity gain than that provided by a simple practical design. Computational examples illustrate the effectiveness of adding additional elements to the optimal array and the relationship between aperture size or the description of the impinging field and the array performance.

A synthesis procedure is proposed which uses genetic algorithm optimization to optimally place a reduced number of dipoles. The results from this procedure demonstrate that using the framework in conjunction with optimization strategies can lead to practical designs which perform well relative to the upper performance bound. Finally a novel array architecture is proposed where subsets of antennas are combined together into super-elements which are then combined in the same manner as the optimal array. The simplifications that result from the genetically optimized small array or the super-element array provide a design options which are feasible in many communication applications.

ACKNOWLEDGMENTS

First I would like to thank my wife Kirsten for her support and sacrifice which made the completion of this research possible. I would also like to thank my daughter Alexis for sacrificing time with me so I could complete this work. I would like to thank my parents for their support. Finally I would like to thank my adviser, Michael Jensen for all the ideas and encouragement he gave me through the entire research process.

Table of Contents

List of Tables

List of Figures

Chapter 1

Introduction

The increasing demand for wireless delivery of all forms of content has necessitated the development of techniques that allow high data rate wireless communication on limited available frequency spectrum. While a variety of techniques exist for increasing the spectral efficiency of wireless links, the use of multiple-input multiple-output (MIMO) technology in multipath propagation environments is arguably the most effective technique. This type of communication uses multiple antennas at both the transmitter and the receiver to exploit the complex spatial structure of the multipath propagation, enabling dramatic increases in achievable data rates.

Naturally, the performance of MIMO communication depends critically on the ability of the antenna arrays to effectively interact with the impinging field. Analyzing the performance of specific antenna configurations in a propagation channel for any type of multi-antenna system has become a relatively straightforward task thanks to a large number of studies on this subject [1, 2] (also see [3] for references to a large number of papers on this topic). The understanding gained by this prior work has led to the common practice among antenna designers of seeking antenna arrays whose element radiation patterns are nearly orthogonal, as such a criterion leads to good performance in multi-antenna systems under specific assumptions regarding the propagation environment [2].

While this rule-of-thumb has been useful in antenna synthesis work, its applicability is limited to scenarios where the multipath is equally likely to arrive from (or depart into) all angles. What is therefore needed is a generalization of this concept which can specify optimal antenna radiation characteristics given basic information about the propagation environment. This allows determination of the performance

of a practical array relative to the achievable performance and facilitates synthesis of antennas that approach the optimal bound. Recently, some work has appeared on this topic, where optimal antenna characteristics can be determined for MIMO systems operating in a specific propagation environment [4]-[7], although in reality the resulting antenna radiation behavior is a by-product of an effort to determine the antenna-independent capacity bound of a propagation channel. While these methods are intriguing, they necessarily consider the transmit and receive antenna characteristics together (i.e. the designs are interdependent), and the resulting antenna properties are optimal for the specific propagation channel considered. An effective and practical approach for antenna synthesis should rely only on average propagation behavior at one end of the link.

1.1 Thesis Contributions

This thesis directly addresses the problem of defining optimal antenna characteristics for MIMO systems through a series of related contributions. Those contributions can be summarized as follows:

1. A method for determining optimal radiation characteristics based on stochastic characteristics of the propagation environment at either the transmit or receive end of the link along with an aperture within which the antenna must reside. The approach is based on ensuring that the radiation patterns are eigenfunctions of the spatial correlation operator and provides the optimal antenna current distributions.

2. A synthesis procedure for the design of an array consisting of a small number of dipoles that performs well with reference to the optimal performance bound. This synthesis uses genetic algorithm optimization to select the placement of the dipoles in the array.

3. A novel array architecture which provides simplified implementation relative to the optimal array. This involves combining sets of antennas into what are called

super-elements which are then optimally combined to form the array. Multiple methods are proposed for determining the super-element weightings.

1.2 Thesis Organization

The remainder of this thesis is organized as follows. Chapter 2 discusses the background research that is important in understanding the concepts and ideas referenced in subsequent chapters. This includes a discussion on the importance of array design in achieving quality MIMO performance. In Chapter 3 the derivation of the optimal antenna array is given. Several computational examples are explored in Chapter 4. These examples facilitate discussion on supergain, mutual coupling, and the effective number of spatial degrees of freedom that are present for a given aperture size.

To explore what is achievable using practical array topologies, two different techniques are explored. The first of these which also serves as a synthesis procedure uses genetic algorithm [8] optimization to optimally place a reduced number of dipoles. This approach which is discussed in Chapter 5 is a practical synthesis procedure which can be easily implemented for any array size. Chapter 6 presents the second practical array architecture which combines disjoint subsets of antennas into super-elements. Chapter 7 concludes the research discussed in this thesis as well as suggests future related work.

Chapter 2

Background Research

MIMO uses multiple antennas at the transmitter and receiver to create parallel, independent channels in a multipath propagation environment. These spatial channels allow the simultaneous transmission of multiple streams of data over the same frequency band and at the same time. The signals are then decoupled at the receiver to reconstruct the transmitted data. This decoupling at the receiver is achieved through analysis of the channel matrix which consists of the complex gain observed between every transmit and receive antenna pair. The quantity and quality of these spatial channels is dependent on the antenna radiation patterns. This idea motivates simplifying the interdependent transmitter and receiver design problems into two separate array design problems.

2.1 MIMO Model

The research discussed in this paper is based on the assumption that performance of MIMO systems is strongly dependent on the performance of the arrays at each end of a MIMO link. Although subsequent analysis considers the problem to be one of array design, since capacity of a link is the metric used in evaluating communication system performance, it is important explore the relationship between antenna array topology and capacity.

In a MIMO communication system, the vector of complex-baseband (ie sampled matched filter outputs) signals at the receiver is given as

$$\mathbf{y} = \mathbf{H}\mathbf{x} + \boldsymbol{\eta}, \tag{2.1}$$

where $\mathbf{H}$ is the channel matrix, $\mathbf{x}$ is the vector of complex baseband transmit signals, and $\boldsymbol{\eta}$ is vector of additive white Gaussian noise.

For a narrow band system, the channel matrix for a given channel realization is given by

$$H_{mn} = \int_{\Omega_R} \int_{\Omega_T} \overline{\mathbf{e}}_{R,m}(\Omega_R) \cdot \overline{\overline{\mathbf{G}}}_P(\Omega_R, \Omega_T) \cdot \overline{\mathbf{e}}_{T,n}(\Omega_T)\ d\Omega_R\ d\Omega_T, \tag{2.2}$$

where Ω_T and Ω_R are solid angle coordinates relative to the transmit or receive array, $\overline{\mathbf{e}}_{R,m}$ is the radiation pattern for the mth receive element, and $\overline{\mathbf{e}}_{T,n}$ is the radiation pattern for the nth transmit element. $\overline{\overline{\mathbf{G}}}_P(\Omega_R, \Omega_T)$ is a dyadic function which represents the relationship between the field radiated by the transmitter in direction Ω_T to the field impinging on the receiver in direction Ω_R. One realistic model for $\overline{\overline{\mathbf{G}}}_P(\Omega_R, \Omega_T)$ is

$$\overline{\overline{\mathbf{G}}}_P(\Omega_R, \Omega_T) = \sum_{l=0}^{L-1} \overline{\overline{\boldsymbol{\beta}}}_l \delta(\Omega_T - \Omega_{T,l}) \delta(\Omega_R - \Omega_{R,l}), \tag{2.3}$$

where δ is a Dirac delta function. This models L discrete paths from the transmitter to receiver each with dyadic complex gain $\overline{\overline{\boldsymbol{\beta}}}_l$. When this model is used, the channel matrix for a given link becomes

$$H_{mn} = \sum_{l=0}^{L-1} \overline{\mathbf{e}}_{R,m}(\Omega_{R,l}) \cdot \overline{\overline{\boldsymbol{\beta}}}_l \cdot \overline{\mathbf{e}}_{T,n}(\Omega_{T,l}). \tag{2.4}$$

The capacity of a MIMO link is found through analysis of the channel matrix $\mathbf{H}$ using the water filling method [9]. The channel matrix can be expressed using the singular value decomposition as $\mathbf{H} = \mathbf{USV}^\dagger$ where $\{\cdot\}^\dagger$ is the conjugate transpose. The singular values in $\mathbf{S}$ determine the number of spatial channels that can be utilized for a given transmit power as well as the capacity of that channel. To provide credibility to the assertion that MIMO capacity is heavily dependent on the topology of the antenna array, an example is given in which two array topologies are compared. Both arrays consist of 4 Hertzian dipoles oriented in the $\hat{z}$ direction. In the first array, four dipoles are spaced by $\lambda/3$ so that the linear array has length λ,

where λ is the free-space wavelength. In the second array, four dipoles are placed at the corners of a square of side length $\lambda/2$. In the channel model, $\Omega_{R,l}$ and $\Omega_{T,l}$ are restricted to the horizontal plane and are uniformly distributed in ϕ. Averaging the water filling capacity [10] over several trials results in the behavior shown in Figure 2.1. The different configurations plotted are when both the transmitter and the receiver are a linear array, when both are a grid array, or when the transmitter is a grid array and the receiver is a linear array. The x axis is in SNR_t which is the ratio of total transmit power to the noise power received by a single element. These results demonstrate that in the MIMO link modeled here, a grid antenna is superior to a linear antenna. From these results, it is clear that the capacity is dependent on the topology of the antenna array.

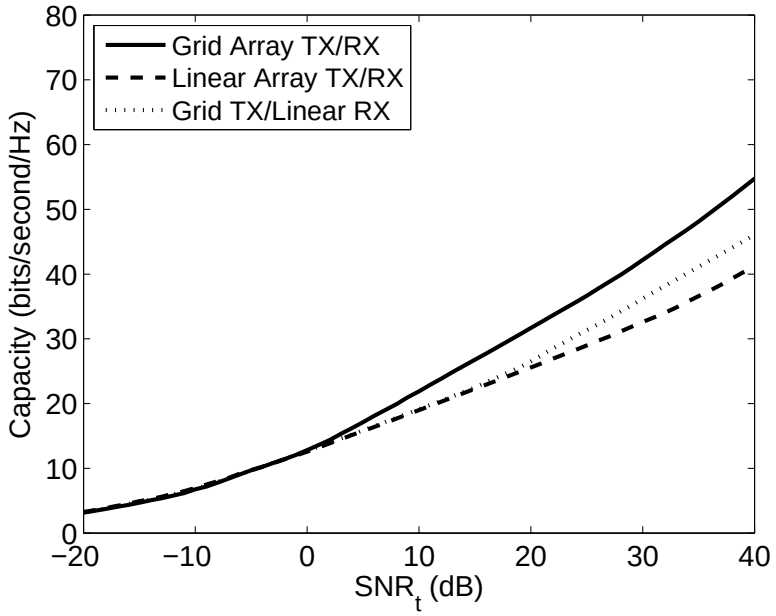

Figure 2.1: The channel capacity using the water filling solution for different array topologies.

2.1.1 Correlation

The ability for the system to utilize these spatial channels is dependent on the channel state information (CSI) at the transmitter. In the case where the transmitter has current and accurate knowledge of the channel matrix, called perfect CSI, maximum capacity for the MIMO channel can be achieved. In fading environments, continuously maintaining perfect CSI at the transmitter is difficult. In light of this, analysis has been done to determine what performance can be achieved if the transmitter knows nothing about the channel. Marzetta and Hochwald [11] showed that in a fast fading environment with spatially white fading, the system capacity is degraded. The assumption of spatially white fading is often overly pessimistic because when the receive array elements are closely spaced, the receive signals will be correlated.

Adopting a new correlation model, Jafar and Goldstein [12] later showed that spatially correlated fading makes improvement in performance is possible. With this approach, the transmitter chooses the antenna weighting and power allocation based on the eigenvectors and eigenvalues of the transmit antenna spatial covariance matrix. This obviously requires that the transmit antenna have access to the transmit covariance matrix. The advantage of this approach is that although the channel matrix might be changing rapidly, the covariance matrix will change slowly so that feedback can occur less frequently.

This covariance matrix is computed as follows for an N transmitter and M receiver system. Given an $M \times N$ channel matrix $\mathbf{H}$, the $MN \times MN$ covariance matrix $\mathbf{R} = \mathrm{E}\left\{\mathrm{Vec}(\mathbf{H})\mathrm{Vec}(\mathbf{H})^{\dagger}\right\}$ where $\mathrm{E}\{\cdot\}$ represents an expectation and $\mathrm{Vec}(\cdot)$ indicates stacking the columns of an $M \times N$ matrix into an $MN \times 1$ vector. The covariance matrix $\mathbf{R}$ can be shown to be $\mathbf{R} = \mathbf{R}^r \otimes \mathbf{R}^t$ where $\mathbf{R}^r$ and $\mathbf{R}^t$ are the receive and transmit covariance matrices respectively and $\otimes$ is the Kronecker product. Jafar and Goldsmith [12] then conclude that the capacity of a MIMO link is dependent on the eigenvalues of $\mathbf{R}^t$, although this conclusion also applies to $\mathbf{R}^r$. This conclusion means that maximizing the eigenvalues of the receive or transmit covariance matrices will result in improved capacity.

Because MIMO communication is dependent on the relationships between all transmit and receive antenna pairs, evaluating a MIMO link should include of both transmitter and receiver. However the Kronecker nature of the covariance matrix and the dependence of capacity on the eigenvalues of the correlation matrix make considering one side of the communication system a valid approach.

2.2 Diversity Gain

In considering only one side of the communication system, the problem simplifies to an antenna array design problem; as a result array analysis machinery can be employed. Diversity gain will be used in this work to compare the performance of the antenna arrays.

In most propagation environments, the signal received by an antenna can vary widely in phase and magnitude as a result of multipath. The resulting wireless link will at times be in a fade where received power is greatly reduced. To overcome this, multiple receive antennas can be used. This is effective because it is unlikely that all the antennas are simultaneously in a fade. In diversity systems, the signals from the several antennas are combined to increase the resulting signal integrity. The method for combining the receive signals which results in optimal performance is called maximal ratio combining. Maximal ratio combining scales all the incoming signals by a complex exponential to shift phase and adjust weighting to maximize signal-to-noise ratio (SNR). The results in this paper assume the use of maximal ratio combining.

The electric field observed by a single receiver is often modeled using a Rayleigh probability density function (PDF). If N_t independent signals are received, each with the same SNR, the cumulative distribution function (CDF) of the SNR for the combined signal given in [1] is

$$P(\gamma \leq x) = 1 - e^{-x/\Gamma} \sum_{m=1}^{N_t} \frac{(x/\Gamma)^{m-1}}{(m-1)!}, \tag{2.5}$$

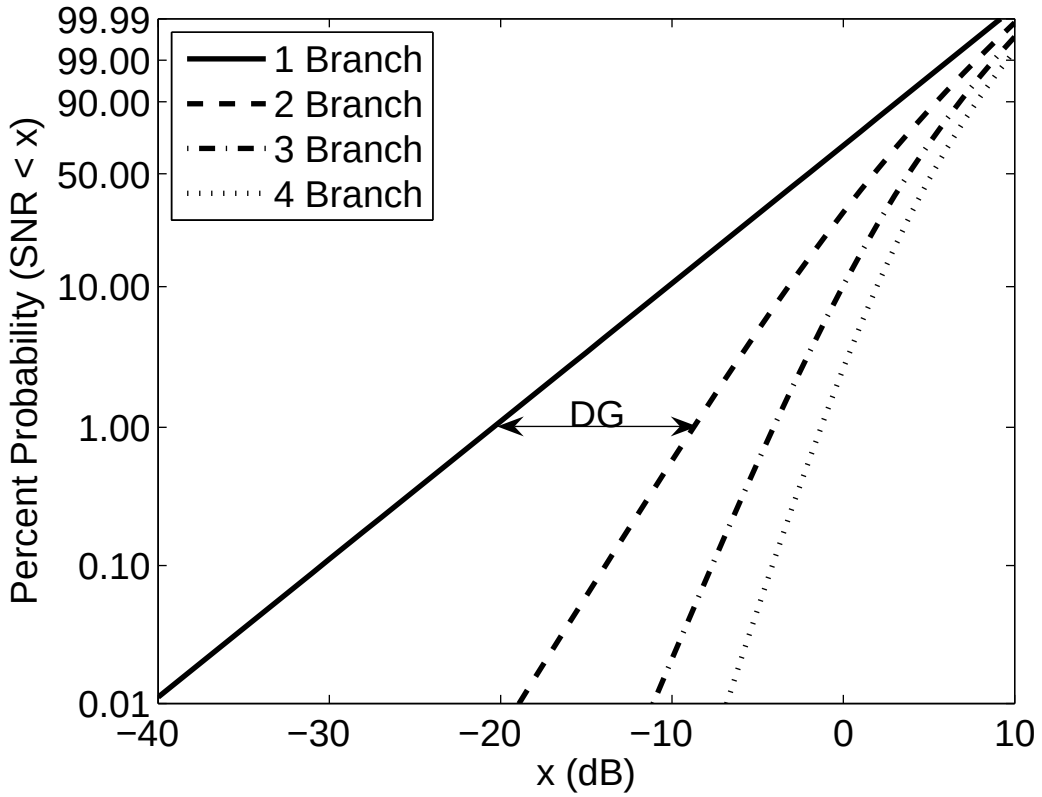

Figure 2.2: Diversity gain is the improvement in SNR that is achieved with a given probability of failure.

where γ is the instantaneous receive SNR for mean SNR Γ. Figure 2.2 plots this CDF for N_t ranging from one to four antennas and where Γ has been normalized to unity. Diversity gain, labeled DG in the figure, is the improvement in SNR that can be observed for a given probability of failure. The figure shows that by adding a second independent branch results in a performance improvement of 11.7 dB over the single branch case for a 1.0% probability of failure. The results given throughout this thesis assume this value. If the branches each have a unique SNR then the CDF can be expressed as

$$P(\gamma \leq x) = \sum_{m=1}^{N_t} \frac{1}{\epsilon_m}(1 - e^{-x/\Gamma_m}) \tag{2.6}$$

and

$$\epsilon_m = \prod_{k=1 k \neq m}^{N_t} 1 - \frac{\Gamma_k}{\Gamma_m}, \tag{2.7}$$

where Γ_k is the SNR for the kth branch. The results form [1] demonstrate that the eigenvalues of the spatial covariance for the array (either $\mathbf{R}^r$ or $\mathbf{R}^t$) can be used for the values of Γ_k.

2.3 Supergain

The array directivity is the ratio of power radiated in a given direction relative to that radiated in the same direction by an isotropic antenna radiating the same total power. If array elements destructively interfere and transmit very little power in all directions, the average directivity will still be unity, because both the denominator and numerator are functions of radiated power. If however, the destructive interference in a specific direction is small relative to the interference in all other directions then the array directivity can be artificially high. This phenomenon is known as supergain and has several drawbacks that make the implementation of these modes impractical.

Supergain is often quantified as an array Q. This is defined as

$$Q = \frac{\mathbf{w}^\dagger \mathbf{w}}{\mathbf{w}^\dagger \mathbf{R} \mathbf{w}}, \tag{2.8}$$

where $\{\cdot\}^\dagger$ is the conjugate transpose, $\mathbf{w}$ is a vector of driving currents, and $\mathbf{R}$ is the impedance matrix of the array elements, scaled so that the diagonal is unity. Arrays that have a high Q are often capable of achieving more directivity than is practically achievable for the array electrical size. The Q is large when the radiated power is small relative to the driving current. The prohibitive amounts of ohmic loss that results from these high currents make transmission of an appreciable power using supergain modes difficult. As a result, ohmic loss must be accounted for when optimizing antenna array performance in order to prevent a tendency toward supergain solutions. Another drawback of high Q arrays is that performance is very sensitive to the phase of the driving currents. It should also be mentioned that Q is inversely proportional to bandwidth, suggesting that supergain array weights result in narrowband operation.

Chapter 3

Optimal Antenna Array Definition

While a truly optimal antenna design for MIMO systems in a given propagation environment necessarily involves interdependent synthesis of the transmit and receive arrays, it is much more practical to devise design approaches which treat each end of the link independently. Furthermore, optimal design, at least as previously implemented [4]-[7], uses deterministic propagation information so that the resulting antennas are optimal for a single propagation channel rather than an ensemble of typical channels. To overcome this difficulty, this thesis exploits the connection between diversity and MIMO systems. Specifically, since both MIMO and diversity systems operate on the principle of exploiting the spatial degrees of freedom enabled by the antennas within the propagation environment, antennas designed for good diversity performance generally also yield good MIMO performance [3]. Therefore, using diversity gain as a performance metric allows design of antennas that will perform well in both MIMO and diversity applications while requiring only stochastic information about the channel at only one end of the link. This chapter details the antenna synthesis procedure based on this concept.

3.1 Derivation

The following derivation uses boldface lowercase and uppercase symbols to denote column vectors (vector $\mathbf{x}$ with nth element x_n) and matrices (matrix $\mathbf{A}$ whose element in the mth row and nth column is A_{mn}) respectively. Vectors which represent a electromagnetic field or radiation pattern (where the vector elements correspond to polarization) or coordinates in space have an overbar ($\overline{\mathbf{e}}$), and dyads have two overbars $\left(\overline{\overline{\mathbf{P}}}\right)$.

3.1.1 Signal Covariance

Naturally, optimality of an antenna design will be related to the specific characteristics of the propagation environment, although these characteristics can be specified stochastically [13] to ensure that the final design is appropriate over an ensemble of channels. Consider a scenario where a vector field $\overline{\mathbf{p}}_{\text{inc}}(\Omega)$ impinges on an antenna confined to the volume V, where Ω is used here to represent an angular position in spherical coordinates or $\Omega = (\theta, \phi)$, with θ and ϕ representing respectively elevation and azimuthal angles. It can be assumed that the field is a zero-mean complex Gaussian stochastic process with the field arriving at one angle uncorrelated with that arriving at another angle, or

$$\begin{aligned} \mathrm{E}\left\{\overline{\mathbf{p}}_{\text{inc}}(\Omega)\overline{\mathbf{p}}_{\text{inc}}^{\dagger}(\Omega')\right\} &= \mathrm{E}\left\{\overline{\mathbf{p}}_{\text{inc}}(\Omega)\overline{\mathbf{p}}_{\text{inc}}^{\dagger}(\Omega)\right\}\delta(\Omega-\Omega') && (3.1)\\ &= \overline{\overline{\mathbf{P}}}(\Omega)\delta(\Omega-\Omega'), && (3.2)\end{aligned}$$

where $\mathrm{E}\{\cdot\}$ represents an expectation, $\{\cdot\}^{\dagger}$ is the conjugate transpose, $\delta(\cdot)$ is the Dirac delta function, and $\overline{\overline{\mathbf{P}}}(\Omega)$ is the dyadic power angular spectrum (PAS) of the incident field. Note that this dyadic form is generated by the vector outer product and generally contains the average power in each polarization (diagonal elements) and the cross-correlation of the different polarizations (off-diagonal elements). If the signals received in the different polarizations are uncorrelated, the off-diagonal elements of this dyad are set to zero.

Using this representation of the channel, if $\overline{\mathbf{e}}_m(\Omega)$ represents the open-circuit electric field radiation pattern of the mth receive antenna, then the open-circuit voltage on this antenna can be written as [2]

$$v_m = \varphi \int_{\Omega} \overline{\mathbf{e}}_m(\Omega) \cdot \overline{\mathbf{p}}_{\text{inc}}(\Omega)\ d\Omega, \tag{3.3}$$

where φ is a constant. Since this is simply a linear operation on a zero-mean complex Gaussian random vector, the resulting voltage will also be a zero-mean complex Gaussian random variable [14]. The covariance matrix $\mathbf{R}$ for the antenna terminal

voltage signals has elements

$$\begin{aligned} R_{mp} &= \mathrm{E}\left\{v_m v_p^*\right\} \\ &= |\varphi|^2 \int_{\Omega}\int_{\Omega'} \overline{\mathbf{e}}_m(\Omega)\cdot\ \mathrm{E}\left\{\overline{\mathbf{p}}_{\mathrm{inc}}(\Omega)\overline{\mathbf{p}}_{\mathrm{inc}}^{\dagger}(\Omega')\right\}\cdot\overline{\mathbf{e}}_p^*(\Omega')\ d\Omega\ d\Omega' \\ &= |\varphi|^2 \int_{\Omega} \overline{\mathbf{e}}_m(\Omega)\cdot\overline{\overline{\mathbf{P}}}(\Omega)\cdot\overline{\mathbf{e}}_p^*(\Omega)\ d\Omega, \end{aligned} \tag{3.4}$$

where $\{\cdot\}^*$ is a conjugate and (3.2) is used along with the fact that the radiation patterns are deterministic.

This covariance matrix is a key quantity which contains the information necessary to determine the diversity performance of the antenna array in the environment. In fact, a key contribution of the work reported in [1] is that the diversity gain of a system with correlated antennas may be computed by creating an equivalent system of uncorrelated antennas with the branch gains given by the eigenvalues of the covariance matrix. Optimal antennas, therefore, physically create the scenario where:

1. R_{mm} is large, indicating a large received power and therefore signal-to-noise ratio (SNR) for each antenna.

2. $R_{mp} = 0$ for $m \neq p$, indicating that the radiation patterns are orthogonal with respect to the power angular spectrum of the incident field.

Note that under the condition $\overline{\overline{\mathbf{P}}}(\Omega) = \bar{\bar{\mathbf{I}}}$ (incident power uniformly distributed in angle), item #2 means that the radiation patterns are orthogonal, consistent with traditional design goals.

3.1.2 Basis Expansion

The first step in this formulation is to relate the radiation patterns used in (3.4) to the physical aperture to which the antennas are restricted. Patterns can be defined either by considering radiating currents (transmit perspective) or the weighting of the fields incident on the aperture (receive perspective), with reciprocity being a mechanism to tie these two perspectives into a single framework. While the prior

development of the covariance has used received incident fields, it is arguably more intuitive to define the radiation patterns in terms of radiating currents.

Therefore, consider an electric current distribution residing in our volume V consisting of a weighted sum of vector functions $\bar{\mathbf{j}}_m(\overline{\mathbf{r}})$, with the radiation pattern for the mth current function being given by [15]

$$\overline{\mathbf{e}}_m(\Omega) = \int_V \overline{\overline{\mathbf{G}}}(\Omega, \overline{\mathbf{r}}) \cdot \bar{\mathbf{j}}_m(\overline{\mathbf{r}})\ d\overline{\mathbf{r}}, \tag{3.5}$$

where $\overline{\overline{\mathbf{G}}}(\Omega, \overline{\mathbf{r}})$ is the dyadic Green's function relating the currents to the far-field radiation. To facilitate determination of the current functions which create the optimal radiation patterns, the mth current function is represented as a weighted sum of orthonormal vector basis functions $\overline{\mathbf{f}}_n(\overline{\mathbf{r}})$, or

$$\bar{\mathbf{j}}_m(\overline{\mathbf{r}}) = \sum_n B_{nm} \overline{\mathbf{f}}_n(\overline{\mathbf{r}}), \tag{3.6}$$

where B_{nm} represents an unknown weighting coefficient. Substitution of this expansion into (3.5) yields

$$\overline{\mathbf{e}}_m(\Omega) = \sum_n B_{nm} \int_V \overline{\overline{\mathbf{G}}}(\Omega, \overline{\mathbf{r}}) \overline{\mathbf{f}}_n(\overline{\mathbf{r}})\ d\overline{\mathbf{r}} = \sum_n B_{nm} \overline{\mathbf{z}}_n(\Omega), \tag{3.7}$$

where the function $\overline{\mathbf{z}}_n(\Omega)$ is given by

$$\overline{\mathbf{z}}_n(\Omega) = \int_V \overline{\overline{\mathbf{G}}}(\Omega, \overline{\mathbf{r}}) \cdot \overline{\mathbf{f}}_n(\overline{\mathbf{r}})\ d\overline{\mathbf{r}}. \tag{3.8}$$

Use of this result in (3.4) gives

$$R_{mp} = \sum_n \sum_q B_{nm} \underbrace{\int_\Omega \overline{\mathbf{z}}_n(\Omega) \cdot \overline{\overline{\mathbf{P}}}(\Omega) \cdot \overline{\mathbf{z}}_q^*(\Omega)\ d\Omega}_{C_{nq}} B_{qp}^*, \tag{3.9}$$

or

$$\mathbf{R} = \mathbf{B}^T \mathbf{C} \mathbf{B}^*, \tag{3.10}$$

where $\{\cdot\}^T$ represents a transpose.

3.1.3 Constraints

Before determining the unknown coefficients contained in $\mathbf{B}$, two constraints must first be imposed on the solution. The first is that all radiation patterns should be normalized so that they have the same radiated power, or

$$\frac{1}{2\eta_0} \int \overline{\mathbf{e}}_m^*(\Omega) \cdot \overline{\mathbf{e}}_m(\Omega) \; d\Omega = P_{\text{rad}}, \tag{3.11}$$

where P_{rad} is the desired total radiated power for each pattern and η_0 is the free-space intrinsic impedance. If the vector $\mathbf{b}_m$ represents the mth column of the matrix $\mathbf{B}$, then using (3.7) in (3.11) leads to

$$\mathbf{b}_m^\dagger \mathbf{A} \mathbf{b}_m = P_{\text{rad}}, \tag{3.12}$$

where

$$A_{nq} = \frac{1}{2\eta_0} \int \overline{\mathbf{z}}_n^*(\Omega) \cdot \overline{\mathbf{z}}_q(\Omega) \; d\Omega. \tag{3.13}$$

Recognizing that since the coefficients in $\mathbf{b}_m$ represent currents, the elements of $\mathbf{A}$ effectively represent resistances. In fact, this matrix represents the real part of the full impedance matrix for the array, and therefore contains self and mutual resistances [16].

Next, recognizing that general current distributions can lead to supergain which is impractical [16]-[19], motivating development of a constraint that limits the level of supergain allowable in the solution. If $\mathbf{A}$ is constant along its diagonal, the array Q factor for the mth current function is

$$Q_m = A_{11} \frac{\mathbf{b}_m^\dagger \mathbf{b}_m}{\mathbf{b}_m^\dagger \mathbf{A} \mathbf{b}_m}, \tag{3.14}$$

where we have used A_{11} to normalize the diagonal of $\mathbf{A}$. A substitution (3.12), results in

$$Q_m = \frac{A_{11}}{P_{\text{rad}}} \mathbf{b}_m^\dagger \mathbf{b}_m. \tag{3.15}$$

Specifying the maximum allowable Q factor as Q_T, the constraint on the coefficients becomes

$$\mathbf{b}_m^\dagger \mathbf{b}_m \leq \frac{P_{\text{rad}}}{A_{11}} Q_T. \tag{3.16}$$

3.1.4 Solution

Examining the vector $\mathbf{b}_m$ which maximizes the quadratic $\mathbf{b}_m^T \mathbf{C} \mathbf{b}_m^*$ subject to the constraints (3.12) and (3.16) provides some insight into the problem solution (note that this neglects diagonalization of the covariance). Using a Lagrange multiplier formulation [20] leads to

$$\mathbf{b}_m = \max_{\mathbf{b}_m} \left\{ \mathbf{b}_m^\dagger \mathbf{C}^T \mathbf{b}_m + \gamma_m (P_{\text{rad}} - \mathbf{b}_m^\dagger \mathbf{A} \mathbf{b}_m) + \gamma_m' (Q_T - \mathbf{b}_m^\dagger \mathbf{b}_m) \right\}, \tag{3.17}$$

where γ_m and γ_m' represent Lagrange multipliers and using the fact that the first term is a scalar (so that it can be transposed). This expression can be written using index notation

$$B_{nm} = \arg\max_{B_{nm}} \left\{ \sum_n \sum_q \gamma_m P_{\text{rad}} + \gamma_m' Q_T + B_{qm}^* (C_{nq} - \gamma_m A_{qn} - \gamma_m' \delta_{qn}) B_{nm} \right\}, \tag{3.18}$$

where δ_{pq} is the Kronecker delta function. To find the maximizing solution, we take the complex partial derivative [21] of the argument in (3.24) with respect to B_{pm}^* and set it equal to zero

$$0 = \frac{\partial \left\{ \sum_p \sum_q \gamma_m P_{\text{rad}} + \gamma_m' Q_T + B_{qm}^* (C_{nq} - \gamma_m A_{qn} - \gamma_m' \delta_{qn}) B_{nm} \right\}}{\partial B_{pm}^*} \tag{3.19}$$

$$= \sum_p (C_{np} - \gamma_m A_{pn} - \gamma_m' \delta_{pn}) B_{nm}. \tag{3.20}$$

This optimized solution for all the elements of $\mathbf{b}_m$ can be found simultaneously by solving the expression

$$\left[\mathbf{C}^T - \gamma_m \left(\mathbf{A} + R_{L,m}\mathbf{I}\right)\right] \mathbf{b}_m = 0, \tag{3.21}$$

where $\gamma'_m = \gamma_m R_{L,m}$.

The difficulties with this formulation are that (1) it is difficult to solve for the unknown Lagrange multipliers in closed form and (2) inclusion of the last term in (3.17) forces the array Q factor to equal Q_T, which overconstrains the solution. However, since $\mathbf{A}$ represents the array resistance matrix, the form of (3.21) reveals that $R_{L,m}$ represents the **loss** resistance associated with each basis function [16]. Therefore, to avoid the difficulties with the formulation, an alternate approach is taken by specifying $R_{L,m} = R_L$ as a loss resistance based on physical arguments (such as a specified radiation efficiency for the basis functions) and reformulate the solution.

To simplify the analysis, let $\widehat{\mathbf{A}} = \mathbf{A} + R_L\mathbf{I}$ and, since loss is added,

$$\mathbf{b}_m^\dagger \widehat{\mathbf{A}} \mathbf{b}_m = P_\mathrm{d} \tag{3.22}$$

which represents the power *delivered* to the array. Using the transformation $\mathbf{b}_m = P_\mathrm{d}^{1/2} \widehat{\mathbf{A}}^{-1/2} \mathbf{d}_m$ leads to the maximization problem

$$\mathbf{d}_m = \max_{\mathbf{d}_m} \left\{ P_\mathrm{d} \mathbf{d}_m^\dagger \widehat{\mathbf{A}}^{-1/2} \mathbf{C}^T \widehat{\mathbf{A}}^{-1/2} \mathbf{d}_m + \gamma_m P_\mathrm{d} (1 - \mathbf{d}_m^\dagger \mathbf{d}_m) \right\}. \tag{3.23}$$

Substituting $\widehat{\mathbf{C}} = \widehat{\mathbf{A}}^{-1/2} \mathbf{C}^T \widehat{\mathbf{A}}^{-1/2}$, then using index notation, the expression becomes

$$D_{nm} = \arg\max_{D_{nm}} \left\{ \sum_n \sum_q \gamma_m P_d + D^*_{qm} (P_d \widehat{C_{nq}} - \gamma_m P_d \delta_{qn}) D_{nm} \right\}, \tag{3.24}$$

where D_{nm} is the nth element of column vector $\mathbf{d}_m$. Taking a complex partial derivative with respect to D_{nm} and setting equal to zero results in

$$0 = \frac{\partial \left\{ \sum_n \sum_q \gamma_m P_d + D^*_{qm}(P_d \widehat{C_{nq}} - \gamma_m P_d \delta_{qn}) D_{nm} \right\}}{\partial D^*_{pm}} \tag{3.25}$$

$$= \sum_p (P_d \widehat{C_{np}} - \gamma_m P_d \delta_{pn}) D_{nm}. \tag{3.26}$$

All elements of $\mathbf{d}_m$ can be found simultaneously by solving $(\widehat{\mathbf{C}} - \gamma_m \mathbf{I})\mathbf{d}_m = 0$. This result indicates simply that γ_m is an eigenvalue of $\widehat{\mathbf{C}}$ and, since $\widehat{\mathbf{C}}$ is Hermitian so that it has unitary eigenvectors, $\mathbf{d}_m$ is the corresponding eigenvector. Writing $\widehat{\mathbf{C}} = \boldsymbol{\xi}\boldsymbol{\Lambda}\boldsymbol{\xi}^\dagger$ and $\mathbf{B} = P_{\mathrm{d}}^{1/2}\widehat{\mathbf{A}}^{-1/2}\boldsymbol{\xi}$, where $\boldsymbol{\xi}$ and $\boldsymbol{\Lambda}$ represent respectively the unitary matrix of eigenvectors and diagonal matrix of eigenvalues of $\widehat{\mathbf{C}}$, leads to $\mathbf{R} = P_{\mathrm{d}}\boldsymbol{\Lambda}$ which is diagonal as desired. This is an intriguing result, since the actual Lagrange multiplier problem was not formulated to ensure diagonalization of this matrix. Furthermore, since the covariance represents the M eigenvalues of a matrix, then if the desired system has $\widehat{M} \leq M$ actual antennas, choosing the eigenvectors corresponding to the $\widehat{M}$ largest eigenvalues will lead to the largest possible values of the diagonal covariance matrix elements.

3.1.5 Loss Specification

The loss in the formulation must be specified in a physically meaningful way. If the basis functions used are square-integrable, then one method for specifying the loss is assuming that the currents flow in a material with a conductivity of σ_L. The loss resistance associated with the nth basis is then given by

$$R_{L,n} = \frac{1}{\sigma_L} \int_V |\overline{\mathbf{f}}_n(\overline{\mathbf{r}})|^2 \, d\overline{\mathbf{r}}, \tag{3.27}$$

where $|\cdot|$ represents the vector magnitude.

When the formulation uses dipoles (approximated by delta functions such that (3.27) cannot be used), it is convenient to specify the radiation efficiency of the nth

dipole defined as $\mu_n = A_{nn}/(A_{nn} + R_{L,n})$ so that

$$R_{L,n} = A_{nn}(1/\mu_n - 1). \tag{3.28}$$

For identical dipoles this quantity will be specified as μ_T. In this case, $A_{nn} = A_{11}$ and as a result, $R_{L,n}$ is the same for all n.

3.1.6 Basis Functions

The basis functions used to describe the aperture should be a orthonormal set for the geometry of the aperture chosen. Although not mandatory, it is also useful to choose a set of basis functions that have a closed form far field radiation integral.

The basis functions used in the computational examples discussed in this thesis are Hertzian or half-wave dipoles. In these examples, the optimal array consists of a dense grid of dipoles positioned on a square aperture. An $N \times N$ Hertzian dipole array for a square aperture of side length L is defined as

$$f_n(\Omega) = \delta(x - x_n)\delta(y - y_n), \tag{3.29}$$

where N is the number of dipoles along a grid axis, $n = mN + k$, $y_n = m * L/(N-1)$ and $x_n = k * L/(N-1)$, for $0 \leq m \leq N-1$, $0 \leq k \leq N-1$. Although delta functions shown here are used to model Hertzian dipoles, the positioning will also be used for the optimal arrays analyzed later that are formed using half-wave dipole.

In defining the optimal antenna array there are two potential approaches for basis functions. The first option is to use continuous basis functions like rectangular pulses or Fourier functions. The second option is to model the optimal array using Hertzian dipoles. If a rectangular pulse function array is used, as the number of pulses in the grid gets large, the ratio of ohmic loss to transmit power observed for each pulse gets infinitely small. However, because all basis functions can be seen as resisters in parallel, both performance and total loss remain constant. Conversely, the loss observed for each delta function does not increase as the array becomes increasingly dense. This results in the fact that as the number of dipoles becomes large, the

loss observed for the array gets small. This can be counteracted by decreasing the radiation efficiency of each dipole.

The computational examples considered later define the optimal array using a dense grid of dipoles. This choice was made to facilitate fair and accurate comparison with smaller dipole arrays. This is a fair comparison as long as the radiation efficiency is determined in a meaningful way. For most of the arrays considered in this thesis, the optimal arrays will be defined using either 11×11 or 21×21 dipoles with $\mu_T = .99$.

3.2 Summary

Receive array performance in diversity and MIMO systems has an optimality bound. This bound provides both insight into what is theoretically possible for a given aperture volume and a method comparing the results to the performance of more common array architectures. This facilitates useful design goals and a method for measuring performance against those goals.

Chapter 4

Optimal Antenna Array Results

The purpose of this chapter is to apply the optimal array framework previously developed in a way that provides general insights into the optimal bound and its implications. The previous discussion claimed that ohmic loss should be introduced to regulate supergain solutions. In the first example, the relationship between ohmic loss and supergain suppression is demonstrated more fully. The second example first introduces mutual coupling to the analytical framework and then analyzes the effects of mutual coupling in optimal array design. Through analysis of a uniform PAS, the third example illustrates that there is maximum effective number of modes that can exist for a given aperture size. The fourth example uses the framework developed in the third example to explore the relationship between array performance and the number of modes included in the optimal array for several PAS functions. The final section of this chapter involves a proposal of alternate power constraint that accounts for source and load impedance mismatches.

To simplify the analysis, each example considers a set of vertically-oriented (z-oriented) dipoles arranged in a regular grid in the x-y plane bounded by a square of side length 1λ (unless otherwise noted), where λ represents the free-space wavelength. Each example further assumes that the incident field is vertically polarized with propagation confined to the horizontal plane, or

$$\overline{\overline{\mathbf{P}}}(\Omega) = \begin{bmatrix} P(\phi) & 0 \\ 0 & 0 \end{bmatrix} \delta(\theta - \pi/2), \tag{4.1}$$

leading to the simplification that the vector-dyadic formulation can be reduced to a scalar one.

4.1 Computational Example 1 - Aperture Efficiency and Supergain

This example compares an optimal square aperture to an array formed by placing dipoles at the aperture corners. The power angular spectrum for these simulations is a truncated Gaussian function (Fig. 4.1). The optimal array is defined using a 21×21 Hertzian dipoles grid. This example analyzes the effects of supergain on the array by varying the radiation efficiency of the array. In the first simulation R_L^n has been specified such that each dipole has a radiation efficiency of 99%. This radiation efficiency is also used in the subsequent examples unless otherwise noted.

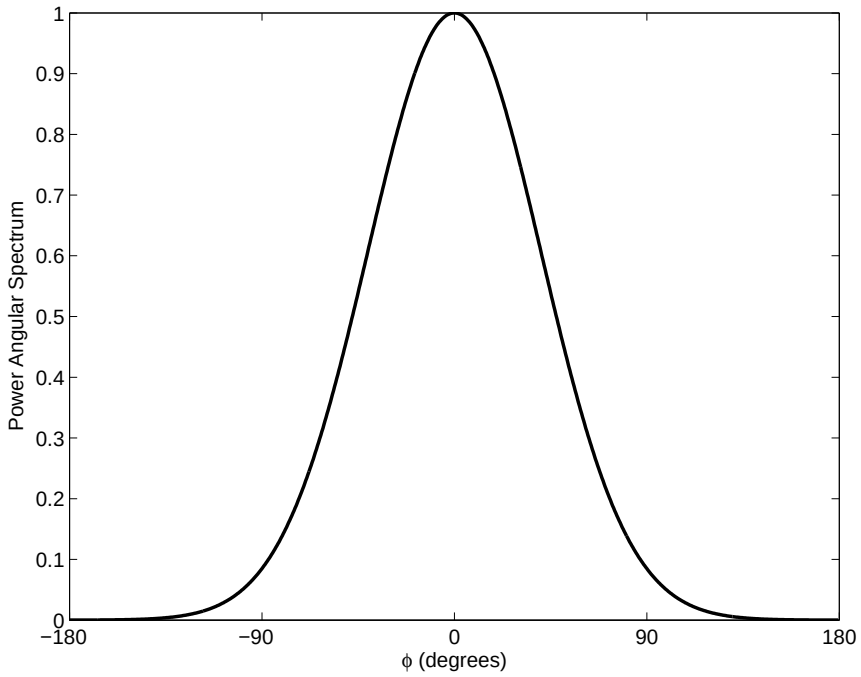

Figure 4.1: Gaussian PAS used in the generation of the optimal radiation patterns in computational example 1

Figure 4.2 shows the current distribution magnitude (in dB) for the dominant four diversity modes for this environment, while Fig. 4.3 shows the resulting radiation pattern magnitudes. For this symmetric and simple PAS, the antenna characteristics show the regularity and symmetry that would be expected. The computation was repeated for the situation where four Hertzian dipoles are situated on the extreme

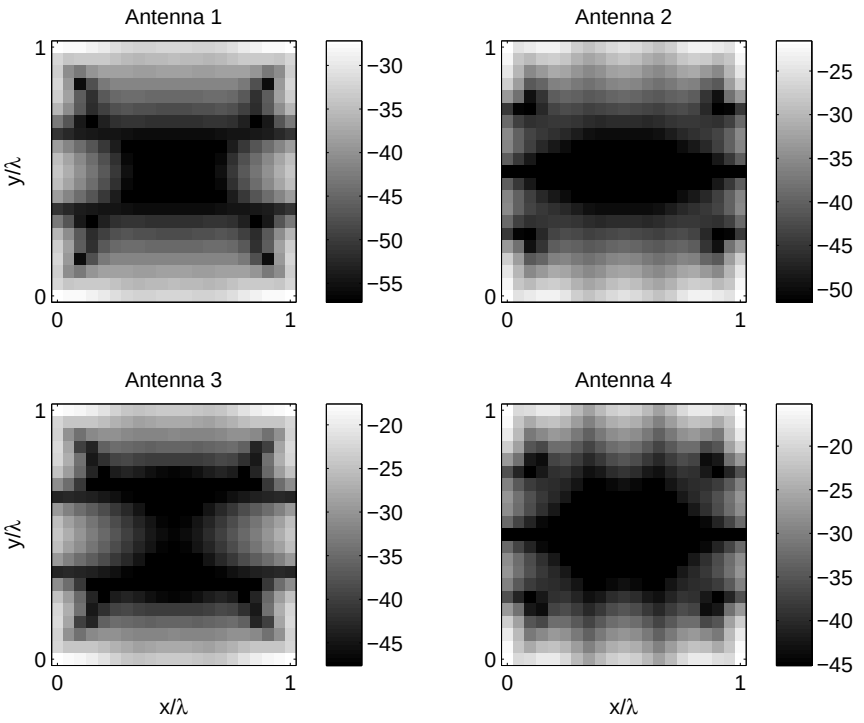

Figure 4.2: The magnitude in dB of the current in the optimal four current distributions for an environment described by a Gaussian PAS when $\mu_T = .99$.

corners of the square array. Using only the dominant four current distributions from the large array results in a diversity gain of 23.3 dB relative to the performance of a single dipole. In contrast, the diversity gain for the four dipoles at the corners is 18.3 dB. This indicates that an optimal design is capable of providing a 5 dB improvement in diversity gain relative to the most simple practical configuration for this environment.

Figures 4.4 and 4.5 show the current and pattern magnitudes for the same computation when the radiation efficiency is increased to 99.999% ($\mu_n = 0.99999$). The current tends to be more concentrated near the aperture edge and much larger in magnitude compared to the case where $\mu_n = 0.99$. In addition the pattern lobes exhibit increased directivity, due to the increased exploitation of supergain excitations. In fact, the Q factor for the dominant mode in this case is 320 times larger than that for the dominant mode obtained with the lower efficiency. Remarkably, however, this increased directivity only results in a 0.5 dB increase in the diversity gain.

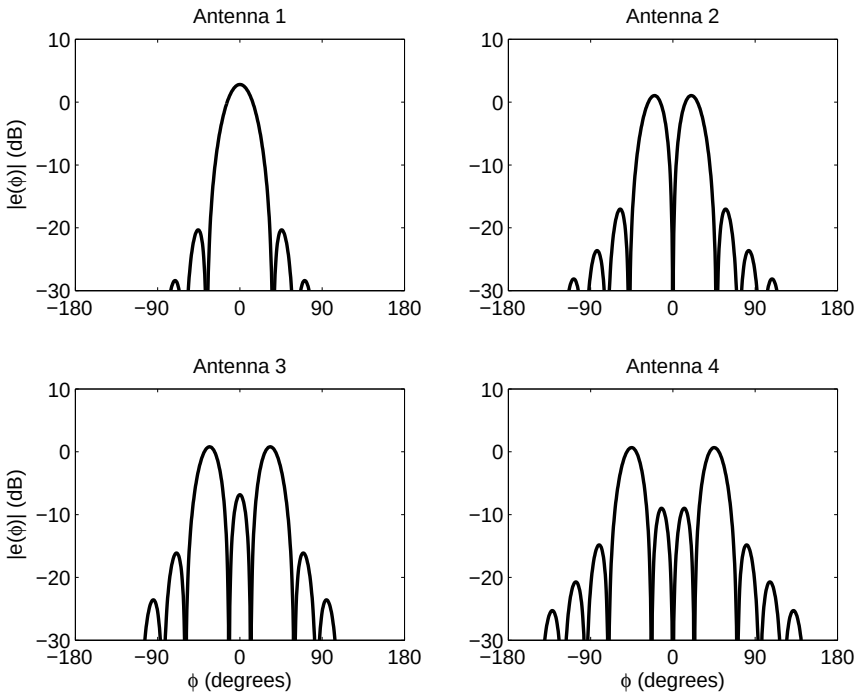

Figure 4.3: Optimal four radiation patterns for an environment described by a Gaussian PAS when $\mu_T = .99$.

4.2 Computational Example 2 - Mutual Coupling

It is also interesting to consider the use of more practical elements as basis functions for the current distribution. This simulation will involve an array of half-wave wire dipole antennas arranged in an 11×11. The radiation pattern for each element in the presence of all other elements terminated in an open circuit is computed using the NEC thin-wire moment method simulator [22], and the resulting patterns are used in the formulation outlined here. Each wire has a diameter of 0.005 wavelengths, and 11 cells per dipole are used in the NEC moment method computation. All subsequent half-wave dipole radiation patterns discussed in this thesis are found using these same parameters. The computations assume the multi-cluster truncated Laplacian distribution shown in Fig. 4.6.

Naturally, full characterization of this system requires also including the mutual impedance of the array elements. However, the results obtained will depend on the assumptions regarding the antenna terminations (i.e. matching network). The

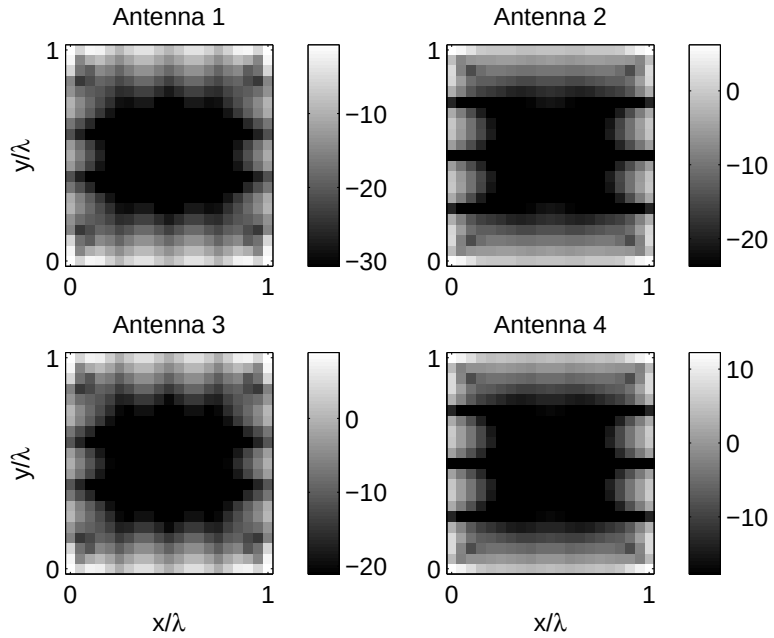

Figure 4.4: The magnitude in dB of the current in the optimal four current distributions for an environment described by a Gaussian PAS when $\mu_T = .99999$.

results obtained here can be used in conjunction with well-established analysis techniques based on network theory to include the impact of impedance effects [23, 24]. Therefore, the following discussion concentrates on the open-circuit characterization so that the results depend only on the patterns.

Figures 4.8 and 4.10 show the current distributions and radiation patterns respectively for this half-wave dipole array. Figures 4.7 and 4.9 show the corresponding results for an 11×11 Hertzian dipole array in the same environment. All computations assume a radiation efficiency of 99%. The resulting diversity gains assuming the four largest communication modes are 22.9 dB for the Hertzian dipole array compared to 23.0 dB for the optimal half-wavelength dipole array. The results are nearly identical, with the slight improvement for the half-wavelength dipoles created by the unique open-circuit patterns exhibited by the coupled dipoles which produces some angle diversity in addition to the space diversity enabled by the array. However, it is important to re-emphasize that the performance of the coupled array of

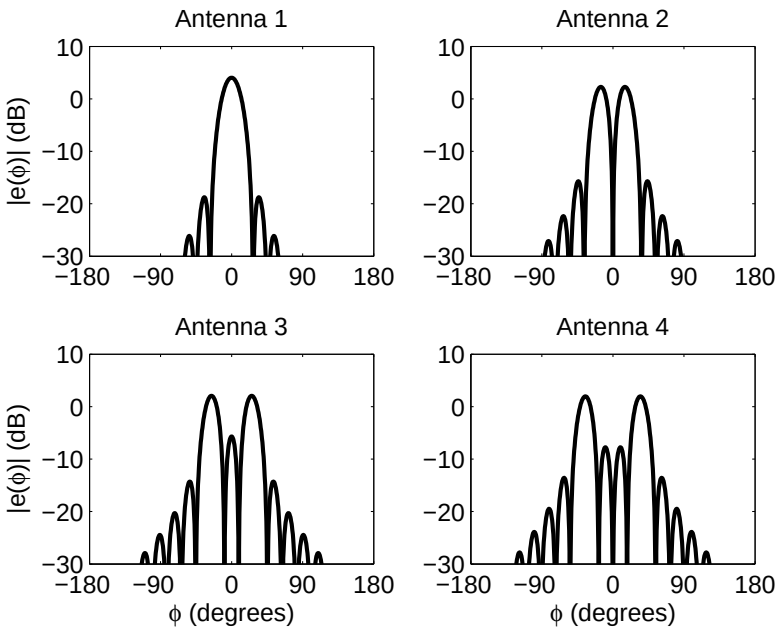

Figure 4.5: Optimal four radiation patterns for an environment described by a Gaussian PAS when $\mu_T = .99999$.

half-wave dipoles will typically degrade significantly if the antennas are attached to a sub-optimal matching network.

4.3 Computational Example 3 - Uniform PAS and the Effective Number of Spatial Degrees of Freedom

In any optimally weighted array, the number of modes which collect appreciable power as well as the performance of each individual mode are dependent on the number of basis functions, the size of the aperture, and the angular spread of the impinging PAS. Increasing aperture size results in improved performance due to an enhanced ability to form beams appropriate for the environment. Increasing the number of basis functions increases array performance by enabling improved approximation to the true optimal radiating currents. For a given aperture size, as the number of basis functions is increased, the power observed by each dominant mode converges to a specific value. As this happens, increasing the number of basis functions indefinitely does not improve array performance by any appreciable amount.

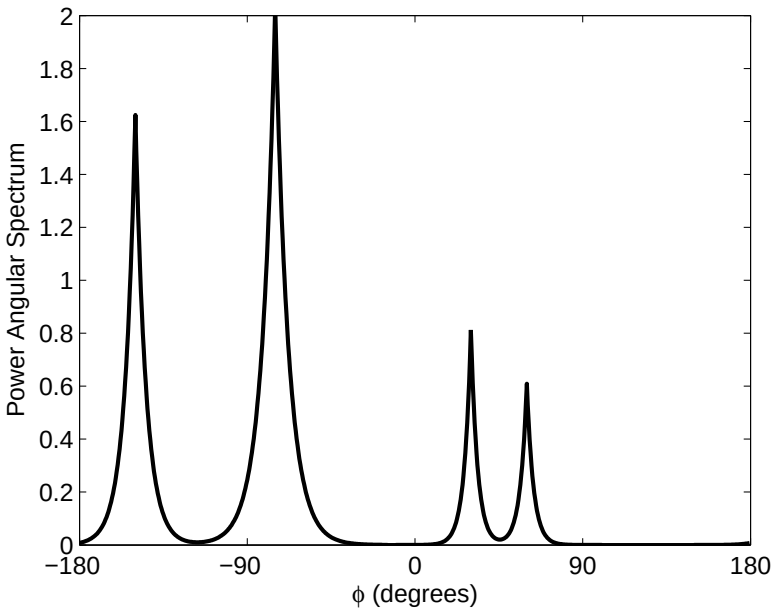

Figure 4.6: Multi-cluster Laplacian power angular spectrum used in the generation of the optimal radiation patterns in computational example 2

For sparse arrays, increasing the number of basis functions facilitates a much better approximation of the true dominant modes and, as a result, much better performance.

To understand the effects of aperture size and number of basis functions on the optimal array performance, it is fruitful to first analyze the performance of an array in the presence of a uniform PAS. This scenario also provides insight into the relationship between basis functions and performance. In this computation, the radiated power P_{rad} rather than the power delivered P_{d} to the lossy array was constrained. Since fixing radiated power is identical to fixing power received from an impinging uniform PAS, the resulting performance is independent of the type or number of basis functions used. An 11×11 dipole grid results in an optimal array with 121 equally dominant array elements. If only four of these 121 optimal elements are selected to form an array, the resulting diversity gain is identical to the diversity gain observed using dipoles at the four corners of the aperture.

Including loss in the simulations changes the results slightly. All modes have degraded performance due to ohmic loss, with the loss observed for each array element

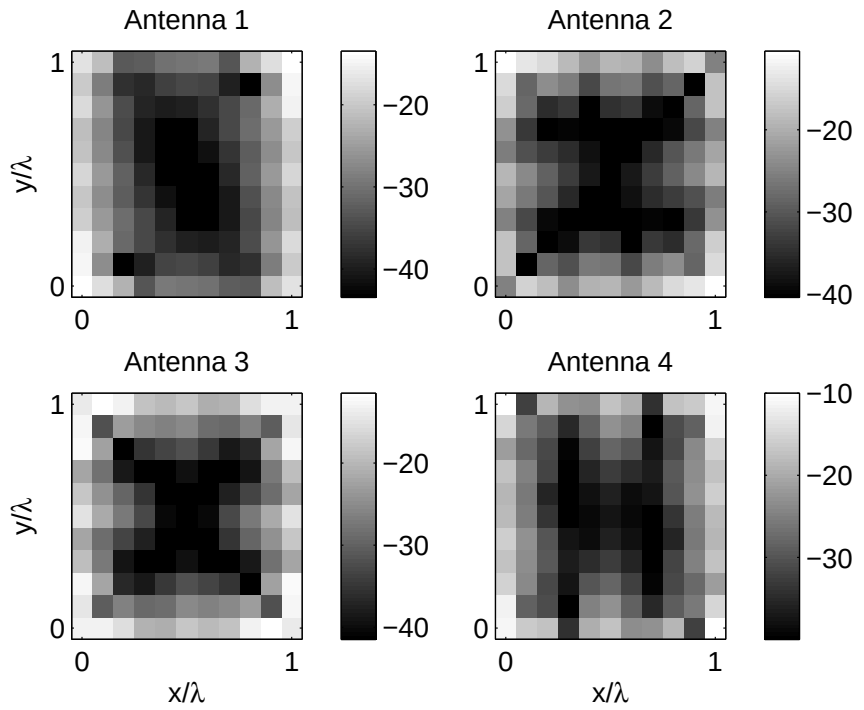

Figure 4.7: The magnitude in dB of the current in the optimal four current distributions for an environment described by a multi-cluster Laplacian PAS using Hertzian dipoles

proportional to the array Q. The example discussed here compares an 11×11 grid of Hertzian dipoles to an array that consists of four Hertzian dipoles placed at the aperture corners. The four optimal radiation patterns shown in Figure 4.11 result in a diversity gain of 19.2 dB. The radiation patterns (Fig. 4.12) resulting from the dipoles at the aperture corners have a diversity gain of 19.1 dB. The difference in performance between the two arrays is entirely based on loss and can be seen as the difference between 4 and 11^2 resistors in parallel.

The performance that results from this example can be expressed as a function of the array Q. This can be done using the delivered power constraint in equation (3.22)

$$P_{\mathrm{d}} = \mathbf{b}_m^{\dagger} \widehat{\mathbf{A}} \mathbf{b}_m. \tag{4.2}$$

First, the delivered power is separated into power dissipated as ohmic loss and power dissipated as radiated signal. Substituting $\widehat{\mathbf{A}} = \mathbf{A} + R_L \mathbf{I}$ and rearranging the equation

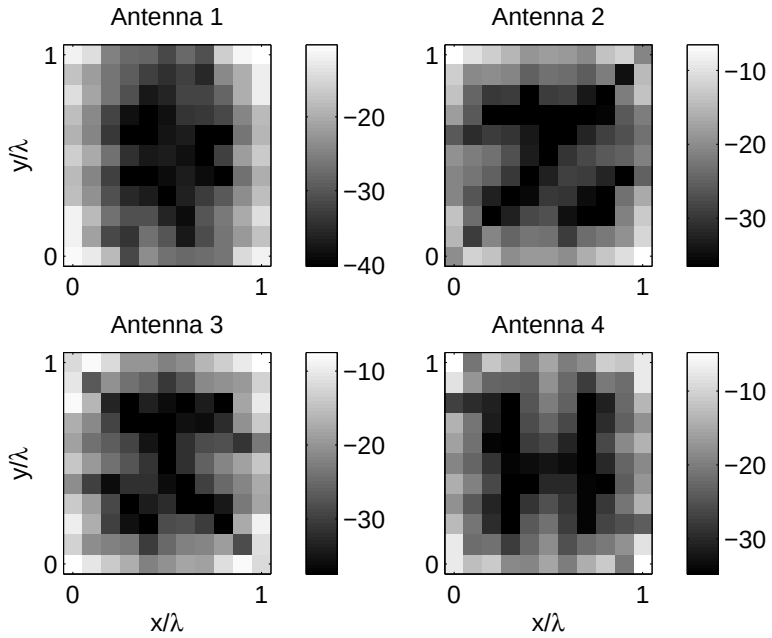

Figure 4.8: The magnitude in dB of the current in the optimal four current distributions for an environment described by a multi-cluster Laplacian PAS using half-wavelength dipoles

results in

$$\frac{P_{\mathrm{d}}}{\mathbf{b}_m^{\dagger}\mathbf{A}\mathbf{b}_m} = 1 + \frac{R_L\mathbf{b}_m^{\dagger}\mathbf{b}_m}{\mathbf{b}_m^{\dagger}\mathbf{A}\mathbf{b}_m}. \tag{4.3}$$

Using equation (3.14) and noting that $\mathbf{b}_m^{\dagger}\mathbf{A}\mathbf{b}_m = P_{\mathrm{rad}}$, the equation simplifies to $P_{\mathrm{d}}/P_{\mathrm{rad}} = 1+R_LQ_m/A_{11}$. Finally, substituting equation (3.28) into this result changes the problem from one in terms of loss resistance to one specified in terms of radiation efficiency. The final expression then becomes

$$P_{\mathrm{rad}} = \frac{P_{\mathrm{d}}}{1 + (1/\mu_n - 1)Q_m}. \tag{4.4}$$

In the presence of a uniform PAS, P_{d} is the same as P_0. As Q_m gets large, it has an inverse relationship with received signal power. This expression shows that, for lossless arrays and a uniform PAS, all modes are equally optimal. The performance dip associated with fewer available antennas then becomes a function of the four element antennas having an array Q that is 15 times larger than that for the 11×11 array. In addition, many of the modes that are not used in the 11×11 array correspond to

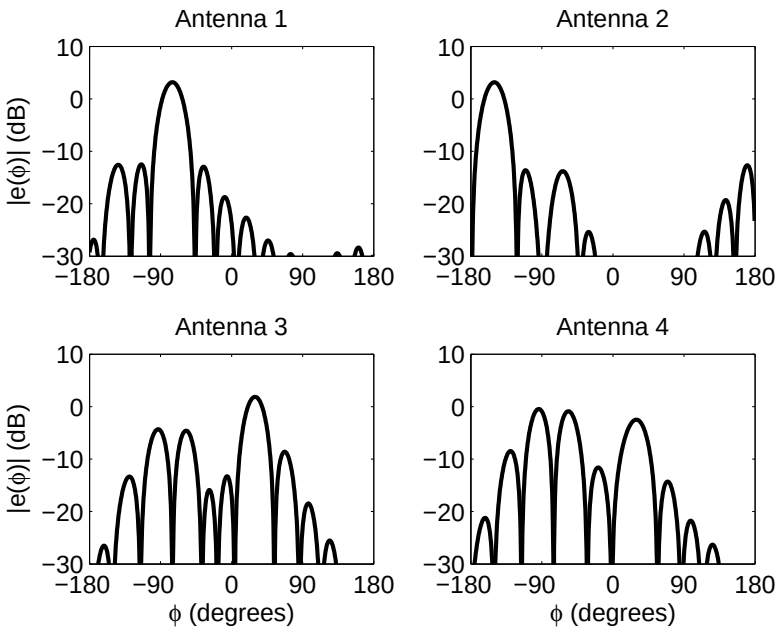

Figure 4.9: Optimal four radiation patterns for a the square aperture in an environment described by a multi-cluster Laplacian PAS using Hertzian dipoles

supergain excitations. The number of modes that are viable increases with the size of the aperture or the radiation efficiency. This property is demonstrated in Figure 4.13.

The diagonal elements of the covariance matrix which represent the received power for each of the optimal modes is shown in Figure 4.13. The number of modes which can be excited to radiate an appreciable power can be considered the spatial degrees of freedom available for defining the optimal modes independent of PAS. For a λ square aperture, there are approximately 15 basis functions that can be used to define the optimal antenna. It is remarkable to see how similar the mode performance is for the 11×11 and 21×21 arrays, with the deviation in performance between the two resulting from the difference between 21^2 and 11^2 resisters in parallel. The two would have identical performance if rectangular pulse functions were used instead of Hertzian dipoles. For a 2λ square aperture this number increases to 26. The exact number of usable modes will increase or decrease as a function of aperture efficiency. The improvement in diversity gain observed by increasing aperture size is merely the

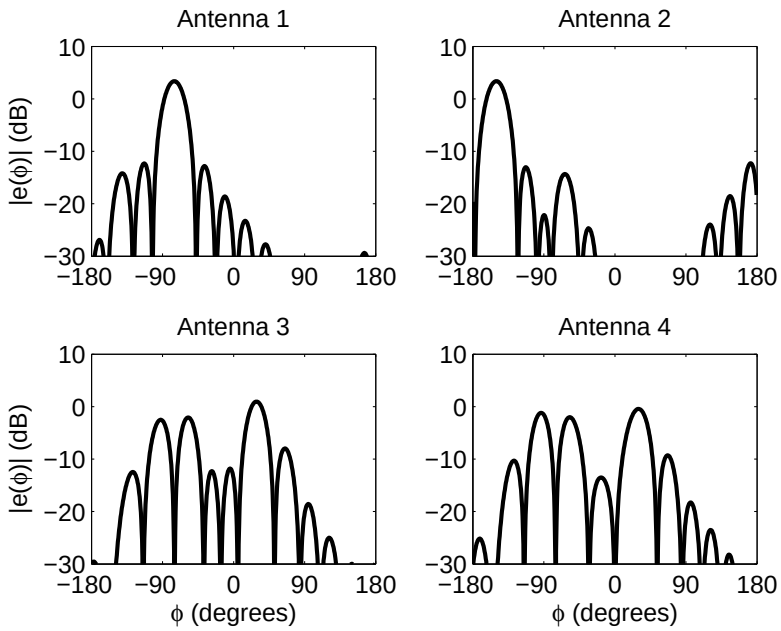

Figure 4.10: Optimal four radiation patterns for a the square aperture in an environment described by a multi-cluster Laplacian PAS using half-wavelength dipoles

result of more basis functions becoming practically available, resulting in a better approximation of the true optimal mode radiation patterns.

4.4 Computational Example 4 - Mode Number PAS Relationship

Another factor that impacts the number of modes with an appreciable power is the angular spread of the impinging signal. If most of the power for an impinging PAS is arriving from a single direction, the number of modes receiving appreciable power will be greatly reduced. The trade off for this is that the received power for the dominant mode will increase as the angular spread of the signal decreases. Figure 4.14 shows the diagonal elements of the covariance matrix relative to P_0 for the optimal modes as a function of mode number and PAS. These results were computed for an 11×11 grid of Hertzian dipoles placed on a square aperture of side length λ. For the uniform PAS, the received power remains constant for the first 15 modes and taper off for higher-order modes. The Laplacian PAS results in the highest power for the dominant mode and the most rapid roll-off for subsequent modes. In this case, the

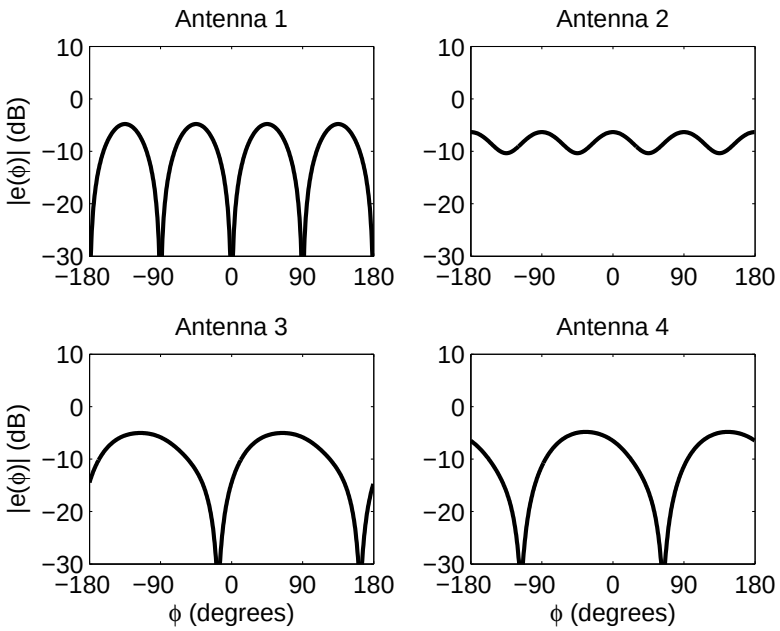

Figure 4.11: Optimal four radiation patterns for environment described by a uniform PAS

four modes with significant received power each lie within the 15 dimensional space corresponding to low Q excitations for the given aperture size. The diversity gain as a function of the number of modes used is plotted in Figure 4.15. For all PASs, the diversity gain eventually levels off as all useful modes are exhausted, although this occurs much later for the uniform PAS than for the other PASs included in the computation.

4.5 Modified Power Constraint

The arrays synthesized in this chapter are based on constraining either power radiated by or delivered to the array. As a result, any reactance associated with the antenna array or a mismatch between the array and feeding network will not be included in the synthesis approach. However, such mismatches are often undesirable in real systems. To account for this, two modifications to the initial formulation are proposed. This formulation solves for the optimal source voltages $\mathbf{v}_m$ rather than the optimal currents. If $\mathbf{Z}_S$ and $\mathbf{Z}_A$ are the source and load impedance matrices

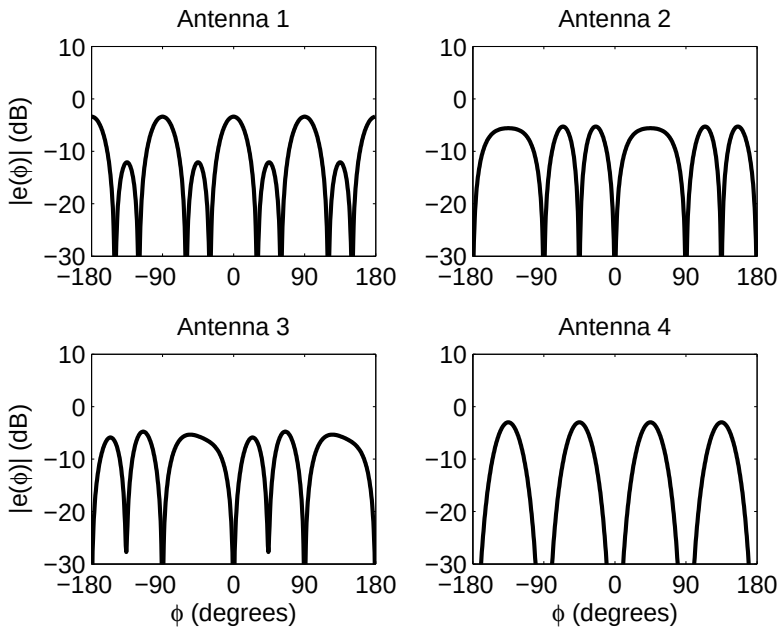

Figure 4.12: Radiation patterns for a optimally weighted dipoles positioned at the aperture corners in an environment described by a uniform PAS

respectively, the covariance matrix $\mathbf{R}$ can be given as

$$\mathbf{R} = \mathbf{V}^T \mathbf{C}_T^T \mathbf{C} \mathbf{C}_T^* \mathbf{V}^*, \tag{4.5}$$

where $\mathbf{C}_T = (\mathbf{Z}_A + \mathbf{Z}_S)^{-1}$ and $\mathbf{C}$ is defined in (3.9). The penalty for impedance effects can be incorporated using the modified power constraint

$$P_0 = \mathbf{v}_m^\dagger \mathbf{A}_M \mathbf{v}_m \tag{4.6}$$

and by defining $\mathbf{A}_M = (\mathbf{Z}_A + \mathbf{Z}_A^\dagger)^{-1}$. This approach constrains the power delivered to the array assuming a conjugate matched load while measuring performance based on the actual load. Most importantly, this reveals that the formulation can be modified to accommodate different desired power constraints. Using simple network theory and by redefining $\mathbf{A}_M$, performance can be optimized for any power constraint.

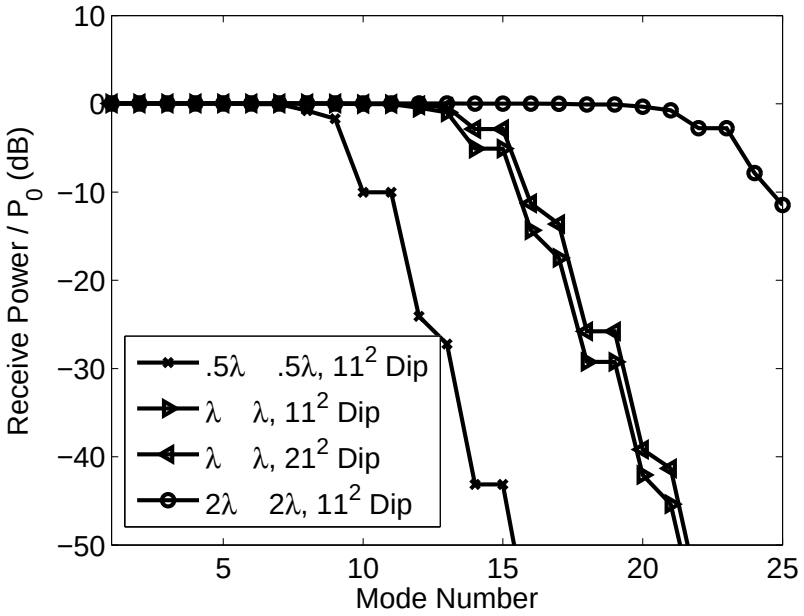

Figure 4.13: The ordered received power of the optimal modes from a uniform PAS for various aperture size and basis function density

4.6 Summary

This section has used several computational examples to outline important aspects of the optimal antenna array formulation. The relationship between antenna efficiency and supergain was discussed, as well as the effect of supergain on array performance. The effects of mutual coupling on array performance were analyzed. In section 4.3, optimal performance was considered for a uniform PAS which gave insight into the spatial degrees of freedom available to construct the optimal array independent of PAS. The final computational example analyzed the effects of angular spread on performance, as well as the number of dominant modes that should be included in an optimal array. Finally, the constraints used in formulating the optimal array were extended to a wider class of array optimization problems by proposing a modified power constraint. This constraint allows the approach outlined here to be adapted to any reasonable design criteria.

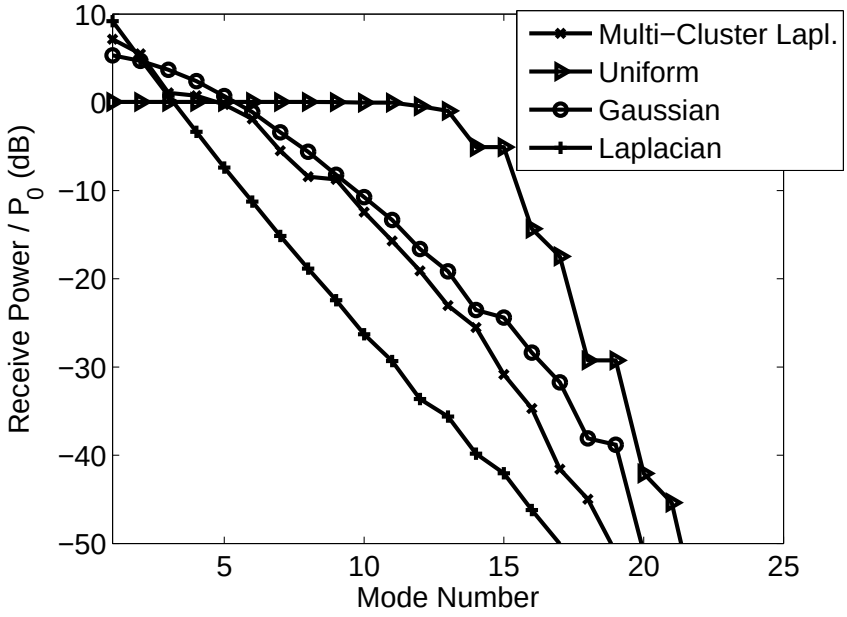

Figure 4.14: The ordered received power of the optimal modes normalized to the receive power of a single dipole for various PASs

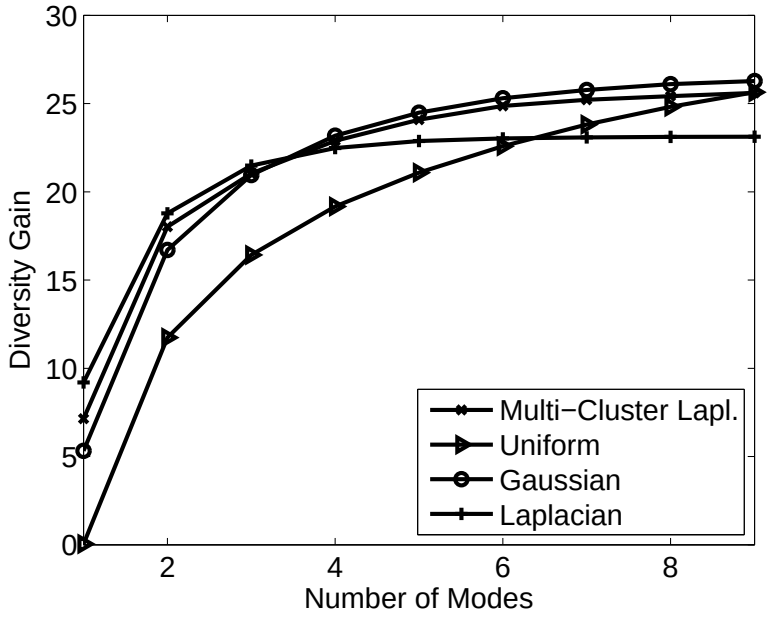

Figure 4.15: The diversity gain of the optimal antenna array as a function of the of number optimal modes in the array

Chapter 5

Genetic Algorithm Optimization

In Chapters 3 and 4, the optimal antennas considered were composed of either 11^2 or 21^2 dipoles arranged in a grid. The complex nature of this array configuration makes forming the optimal array from weighted combinations of 121 dipoles prohibitive for most situations. The relationship between performance and the number of half-wave dipoles placed in a grid is explored in Section 5.1. This leads to the question of what performance can be achieved when antenna placement is not restricted to a grid architecture. The answer to this question is explored using genetic algorithm optimization. An advantage of this approach is that it also provides a useful synthesis procedure for practical array design with near optimal results. The details of the genetic algorithm and the results from the simulations are discussed in Sections 5.2 and 5.3 respectively.

5.1 Performance and the Number of Array Elements

Prior computations have demonstrated that increasing the number of basis functions results in improved performance. The performance of the array cannot be increased to an arbitrary value, but additional basis function elements will result in monotonic convergence to the performance of the true optimal currents. The optimal arrays considered thus far were approximated 11×11 dipole arrays. To explore the validity of this approximation, Figure 5.1 plots the performance of the optimal array for several different PAS representations as the number of half-wave dipoles along a grid axis is increased. The Uniform PAS shows effectively no increase in performance for any array size increase. The other PAS functions considered all converge to performance near the true optimal around 11 or 12 dipoles per axis. The

simulations used for this figure involve a square aperture of side length λ and dipole efficiency of 99%.

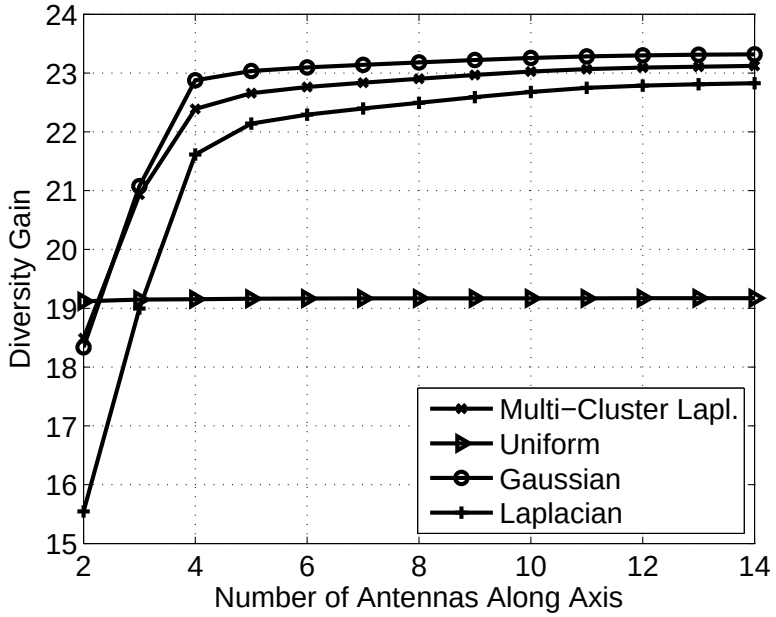

Figure 5.1: The diversity gain of the optimal antenna array as a function of the number half-wave dipoles of along one axis of the grid.

5.2 Genetic Algorithm

Achieving optimal performance for a nonuniform PAS involves at least 121 dipoles. Implementing an optimal array with 121 sensors would be impractical for most communication systems. Reducing the array to a 4×4 array results in sub-optimal performance and in many cases, a 16 element array is still impractical. In order to reduce the number of elements required to achieve near optimal performance, a genetic algorithm(GA) will be used to optimally place a small number of half-wave dipoles. GAs have been used extensively for optimization in electromagnetic problems [25] and have the advantage of an acceptable convergence time coupled with a tendency toward global optimization.

5.2.1 Generic Genetic Algorithm

In a generic genetic algorithm [8], an initial population is created. Each member of the population is described by a chromosome which incorporates all of the attributes being optimized. In the case of an antenna array, this would be the location of each dipole in the array. Each member of the population is given a fitness function based on some performance criteria. Members of the population are selected in pairs to be parents. Selection of parents should favor the more fit members of the population and can occur in a variety of ways. Once parents are selected, the chromosomes of the parents are crossbred to form children. In addition, mutations can be introduced into the children's chromosomes to promote genetic diversity. The children from all selected parent pairs are then either used to replace the entire population or merged with a subset of the parent population. The process of repeating this for a fixed number of generations or until the population converges is called a trial. The solution then comes from the population member with the best performance from either a single or several trials. For discontinuous multidimensional problems like the one in question, trials will rarely result in the same solution, although the best performance from each trial will often be similar.

5.2.2 Genetic Algorithm Implementation

The genetic algorithm implemented here is used to find the optimal half-wave dipole locations for a sparse antenna array. To explore the trade off between array performance and the number of dipoles used in the array, the GA is used to optimize arrays consisting of 4, 6, or 8 half-wave dipoles. The fitness function used was the diversity gain. Since the impinging field only varies in azimuth, only the optimal x and y coordinate are found for each dipole in the array. The dipole locations are constrained so that all dipoles must be within a square of side length λ.

Once a population is initialized, the trial is allowed to run for 125 generations unless all the antenna arrays in the population converged to a single array topology. For each generation, the population is modified using a steady state genetic algorithm, where the least fit portion of the parent population was replaced with a group of

children. The portion of the old population replaced by new children is specified as μ_r. If the population size is 100 and $\mu_r = .8$, then at each generation the 20 most fit members of the old generation are combined with 80 new children to create the new generation. The x and y coordinates for each dipole are represented by a single 7 bit gene (i.e. a 4-element array consists of 8 genes). This approach is a slight deviation from conventional GAs, but results in children that quickly explore the solution space.

Tournament selection is used to determine which members of the population should become parents. This involves randomly selecting several members of the population and then choosing the two fittest members to be parents. This selection approach favors the fitter members more than other approaches and as a result improves convergence. Although other values were explored, in all the simulation results shown here, each tournament consists of five members. Once two parents are selected, crossover occurs on each individual gene (i.e. 8 unique crossovers for a 4-element array) with a probability of 0.7. Once the children have been created, mutations are introduced into the optimization with a probability of .04. To further improve convergence, every 10 generations children are locally optimized with a probability of 0.01 using the Nelder-Mead simplex method. In addition, all mutated children are locally optimized using the same algorithm.

5.3 Genetic Algorithm Results

For all arrays considered here, the diversity gain is found using the four dominant modes of the array. The PAS used for all simulations is a described by a truncated Gaussian pdf (Fig. 4.1). For each set of parameters, the number of trials simulated is fixed by the simulation wall time of 600 hours. When a population size of 20 is used and $\mu_r = .5$, the performance for different array sizes is shown in Figure 5.2. Each array size is analyzed for 20 trials and then the fittest member is chosen from all 20 trials. For the purpose of comparison, the optimal performance bound is plotted as well as 2 common array architectures. The array consisting of 8 antennas along the aperture boundary has a dipole at each corner and a dipole positioned at the midpoint of each edge of the square aperture.

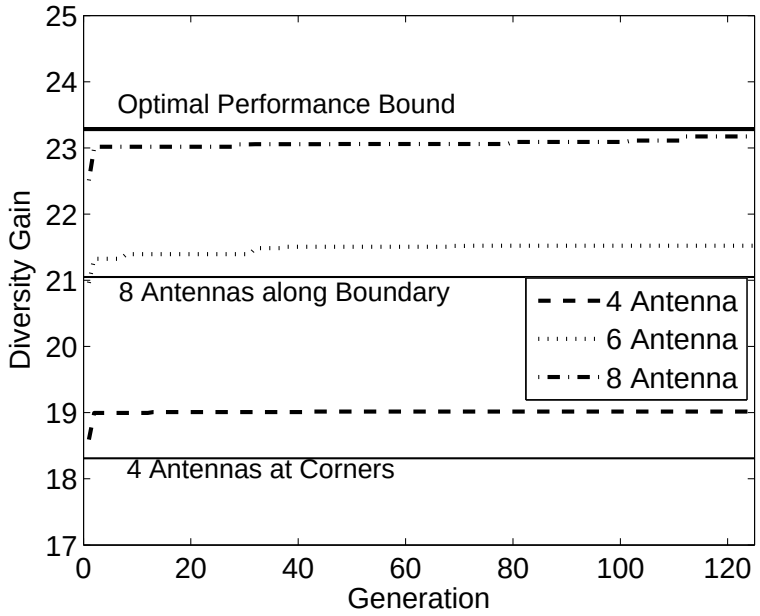

Figure 5.2: The performance of arrays designed using genetic optimization compared to the performance of common array architectures and the optimal bound.

It is surprising to note how well the eight element array performs relative to the optimal performance that can be achieved. Performance is dependent on how well the array can create four patterns that are orthogonal with respect to the PAS. In the four element array, because there are only four degrees of freedom available to create four patterns, the driving currents corresponding to small eigenvalues must be used. As two additional degrees of freedom are added for the six and then two more again for eight element array, the smaller eigenvalues can be ignored and the most effective modes utilized. It is worth noting that the performance of the GA optimized 8 element array performs better than a 7×7 grid of half-wave dipoles.

5.3.1 Parameter Dependent Performance

While the achievable performance is the most significant result of the GA optimization, it is also important to understand how the parameters used in the calculation relate to performance. The parameters that will be explored in detail are

the population size and the portion of the parent population that is replaced each generation with new children.

The first variable discussed is the size of the population which is denoted as P. The simulation time for each trial is dependent on the number of dipoles in the array and the population size. In the case of a 4 dipole array, the 600 hour simulation wall time resulted in 39 trials for $P = 20$, 12 trials for $P = 60$, and 6 trials for $P = 100$. For each trial, the fittest member for each generation determines the performance of that trial. Comparison for the different population sizes occurs for the average trial performance and for the optimal trial performance which consists of the best member of all trials. The average trial performance (Fig. 5.3) is reduced for the smaller population sizes because fewer points of the solution space are explored. The optimal performance for multiple trials is shown in Figure 5.4. These results show that even though the average trial performance is lower for the smaller population, the optimal performance across all trials is approximately the same. Because increasing population size decreases the number of trials that can be completed within the fixed simulation time, the number of trials included in calculating the optimal trial performance for each population size is set by the number of trials that can be run in the fixed time window. In these simulations, the computation time was 1200 hours and $\mu_r = .5$.

In the steady state genetic algorithm used here, for each generation the least fit portion of the population is replaced with an equal number of children. The motivation for this approach is that preserving the fittest members of a population results in more focused exploration of the solution space around the fitter members of the population. The drawback to this approach is the tendency for premature convergence to a local optimum. When each generation is completely replaced by new children or $\mu_r = 1$, the approach is called a generational GA. This method has no tendency toward premature convergence, but the algorithm does not guarantee that if convergence occurs, it will be to the fittest member of the entire trial. In Figure 5.5, the average trial performance of different μ_r values is compared for a four element array with different GA population sizes. Figure 5.6 shows the best

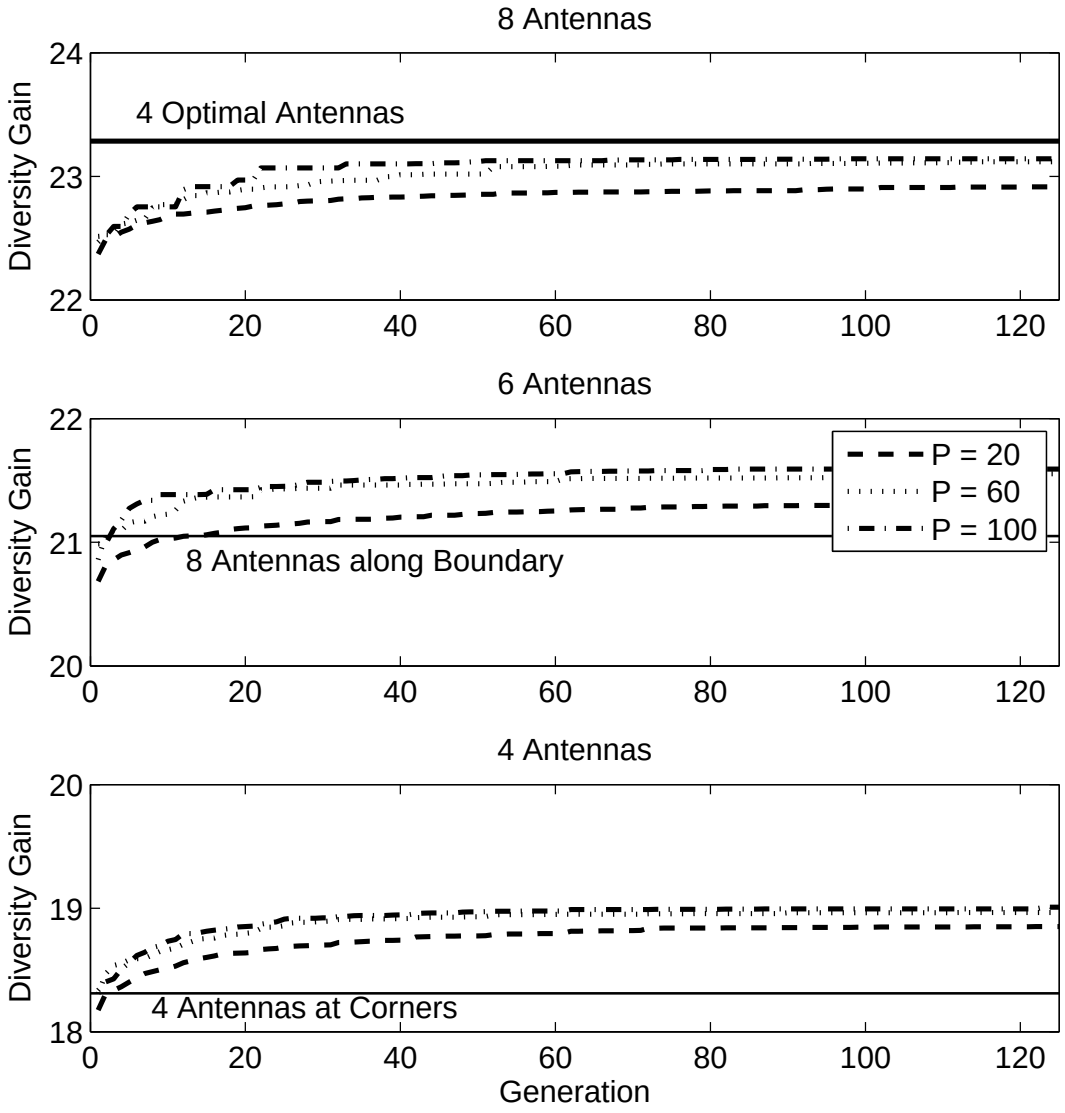

Figure 5.3: The average performance of genetically optimized arrays for different array and population sizes

performance for all trials. It should be mentioned that the trends shown in both these figures is also characteristic of the six and eight element arrays. The average performance is the worst when $\mu_r = 1$ which makes sense because the best members of the previous population are not being carried over. This is especially true for $P = 20$. Even though the average performance is better when the fittest members

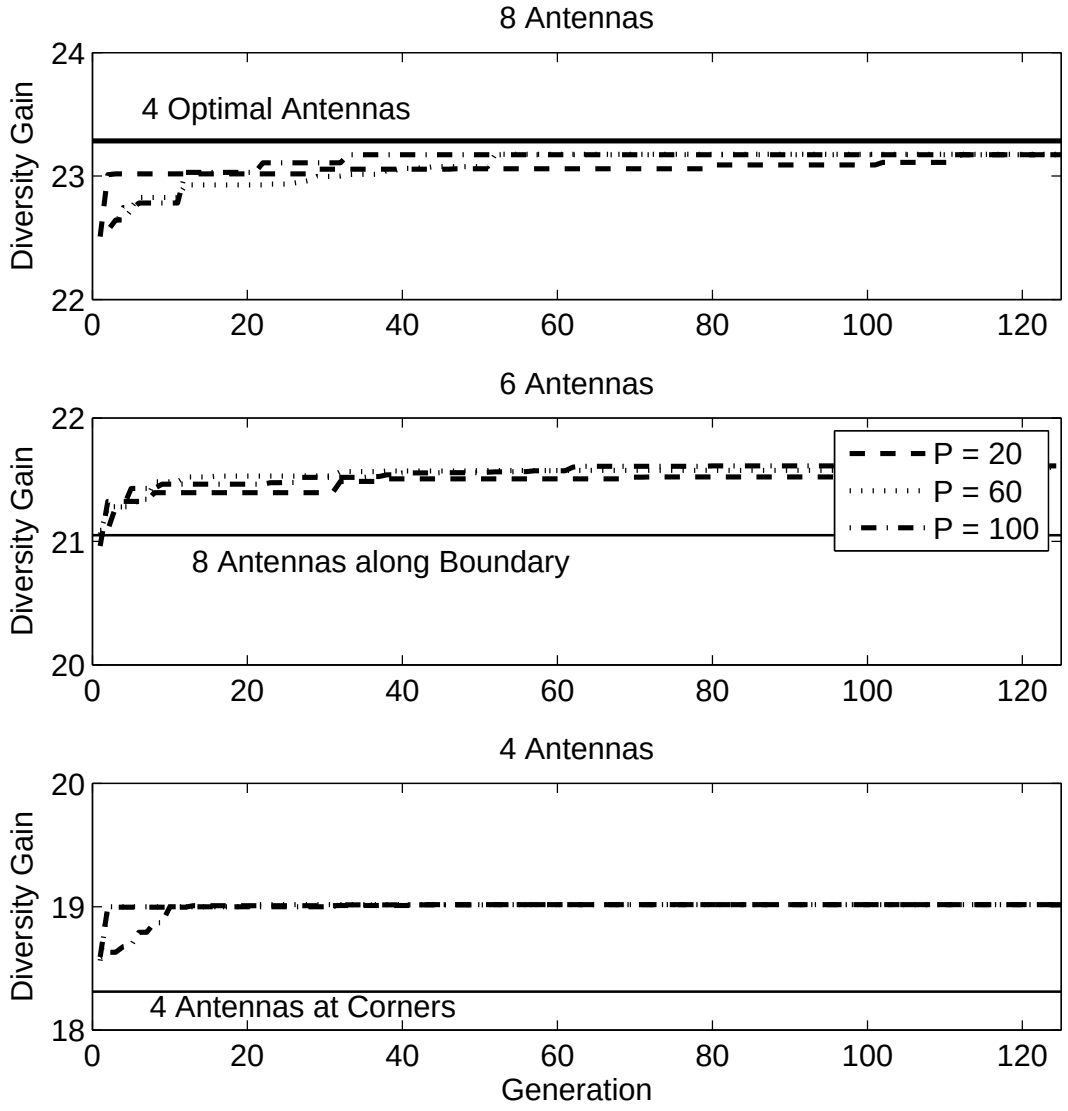

Figure 5.4: The optimal performance of genetically optimized arrays for different array and population sizes

of the population are carried over, the best performance for all trials is not really affected by μ_r.

5.4 Summary

The impractical nature of the dense arrays necessary to achieve optimal performance makes a sparse array with reduced performance appealing. Using a genetic

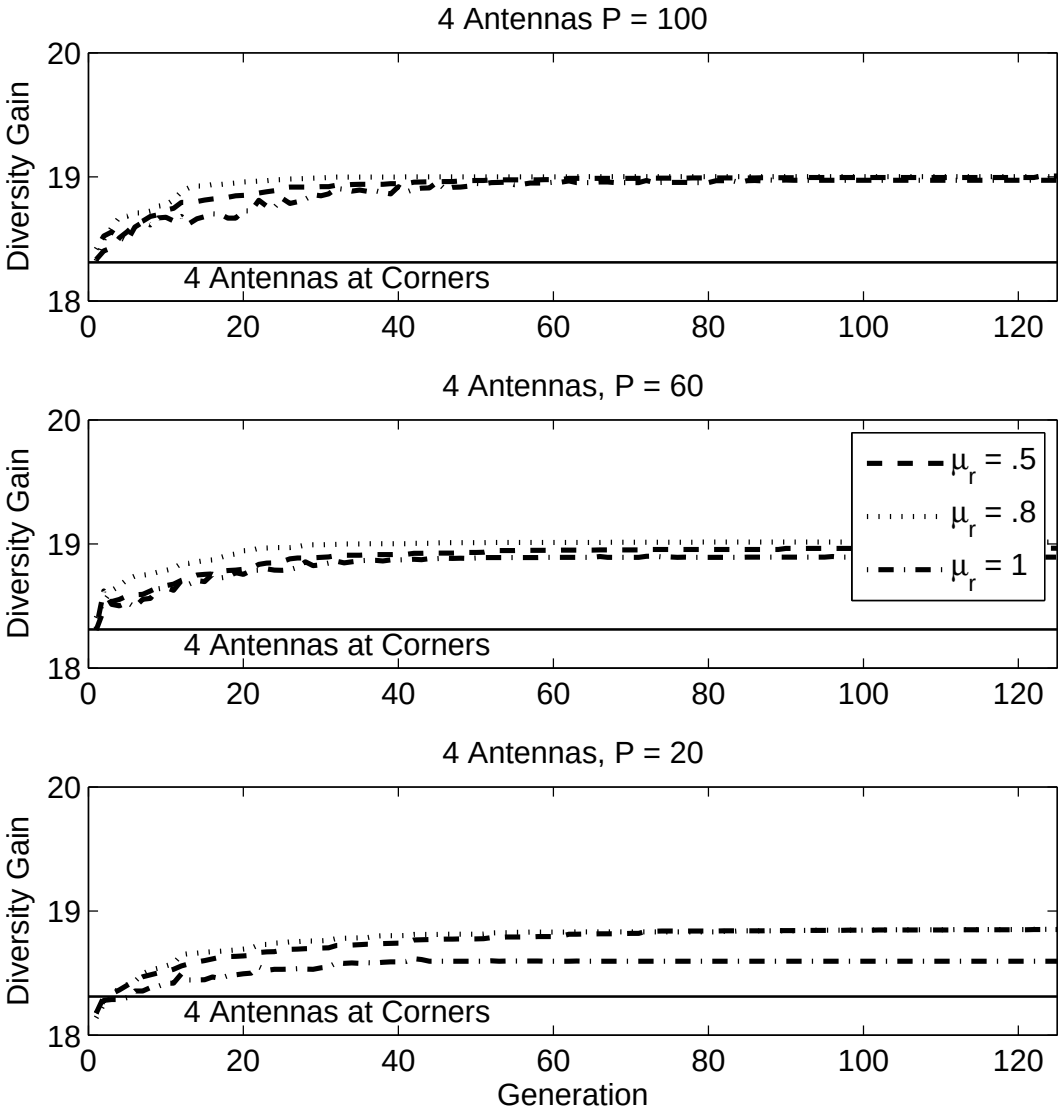

Figure 5.5: The average performance of genetically optimized arrays for a four element array for different population sizes when varying μ_r

algorithm to optimally place the antenna elements can result in good diversity gain performance from a much more sparse array. In the example shown here, near optimal performance was achieved with only eight elements. The average performance of GA trials was found to vary with the parameters used in calculation, but the best per-

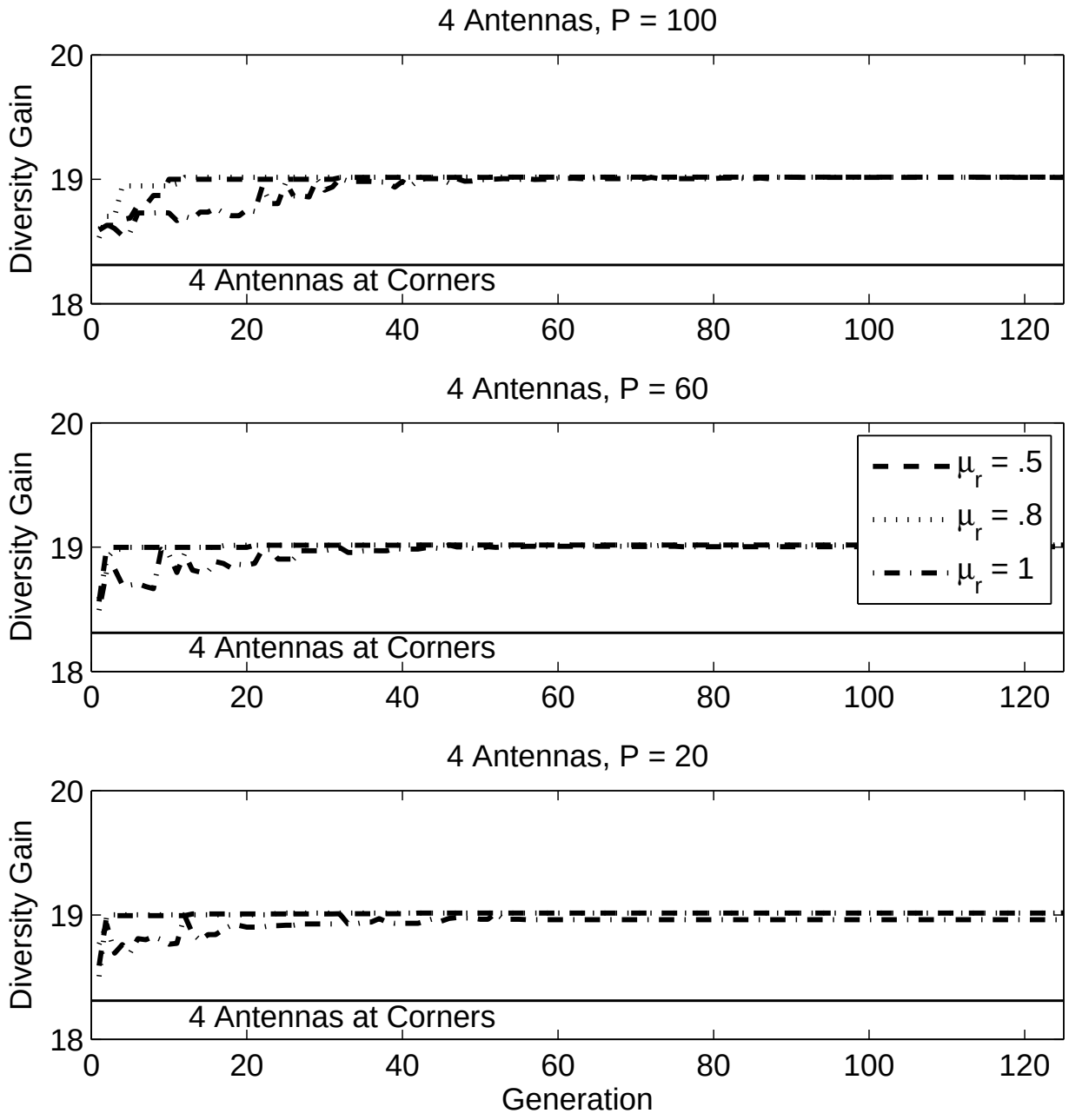

Figure 5.6: The best performance of genetically optimized arrays for a four element array for different population sizes when varying μ_r

formance for several trials of a GA was shown to be relatively unaffected by specific parameters.

Chapter 6

Super Element Arrays

There are two options for implementing an optimal receive array, given that M basis functions are used to form an N element optimal array. The first of these methods performs the weighting and combining of the received signals using analog circuitry. In this approach, for each of the N elements in the optimal array the M basis function receive signals must be scaled by a complex gain and then combined before sampling. The difficulty associated with this technique is that precise analog complex gains must be implemented for MN ports, and then M signals must be summed N times. The advantage of this approach is that only N RF front ends and A/D converters are required. The second option is to have an RF front end with an A/D converter at each of the M basis functions. After digitization, optimal weighting and combining using discrete hardware is feasible. This option is difficult to implement due to both the space and cost associated with the additional RF and sampling hardware. Because each optimal array element has a unique weighting vector, it is necessary that the weighting and combining of the receive signals be completed in a single block either before or after sampling.

The modified approach proposed here facilitates simpler analog combining, and reduces the number of signals that must be sampled. This is accomplished by creating super-elements, each of which is composed of a fixed weighted sum of a subset of the basis functions. The received signal from each super-element is then sampled and combined to form a near-optimal antenna array. If the weightings for the sub-elements can be easily changed real-time and the PAS is time varying, then this approach is superior to optimally placing elements using a genetic algorithm. This is

because the improvements in performance from the super-elements can be sustained because the sub-element weightings can adapt as the PAS changes.

This chapter proposes several potential methods for determining the weightings applied to the sub-elements. Section 6.1 discusses methods of local optimization with super-elements as well as the resulting performance. This section also addresses performance when the analog weightings are limited to phase delays with unit gain. In Section 6.2, two closed form solutions are given which result in near optimal performance and do not require extensive optimization searches.

6.1 Local Optimization

The nature of the optimization makes finding a closed form optimal solution impossible. The several approaches proposed here are attempts to achieve near optimal performance either by a brute force optimization search or by modifying the problem definition to make a closed form solution possible. Because the goal of the proposed architecture is to simplify implementation, the practical advantages and disadvantages associated with the each approach will be discussed.

The first approach is to use local optimization to find the sub-element weightings. Because the relative phase between super-elements is insignificant, the dimensionality of the optimization is $N_s - N_e$, where N_s is the total number of sub-elements and N_e is the number of super-elements. This approach guarantees a local optimum because the optimization algorithm can maximize diversity gain directly. Another advantage of this approach is that if the complex gains can be adjusted in real time, it might be possible to perform the optimization search while the array is in use. Such an approach would require a length initial calibration in which performance would be sub-optimal, but maintaining near optimal performance for a slowly changing PAS would be feasible. If the optimization search cannot be done while the array is in use but the weighting can be changed, then the computationally intensive nature of this approach might be prohibitive.

To compare the performance of the approaches outlined here, a single antenna array configuration will be analyzed in the presence of four different PAS's for each of

the proposed algorithms. The antenna array consists of four super-elements, each of which is composed of three dipoles. These dipoles are spaced equally along the edge of a circle of radius $.5\lambda$ with the first elements having (x,y) coordinate of (0,.5). The super-elements are formed from sets of neighboring dipoles. The local optimization performed here was done using the Nelder-Mead simplex method with the initial values specified using the covariance approach outlined in Section 6.2.1. The problem is an eight dimensional optimization because the complex gain of the first dipole in each super-element can be set to unity. The resulting performance for the different algorithms is shown in Table 6.1. The optimal bound given in this table is computed using of antennas placed in the same locations but with weighting determined without enforcing the super-element constraint. The performance of the locally optimized super-element array is 1.9 dB less than that for the unconstrained array, which is small considering the dramatic simplification in design implementation. The optimal results are also compared to a traditional four element array consisting of dipoles at the corners of a square aperture with side length λ. The four element array has an average diversity gain that is 4.4 dB less than that for the optimal unconstrained twelve element circular array.

Table 6.1: Results if dB for the different super-element weighting algorithms

PAS Description	Optimal Bound	Four Dipoles	Local Optimal	Phase Only	Covariance Approach	Current Approach
Multi-cluster Laplacian	22.29	18.46	20.30	20.03	18.97	19.61
Sinc	21.72	18.24	20.27	20.01	20.08	19.69
Gaussian	22.68	18.31	20.93	20.62	20.38	20.38
Laplacian	21.31	15.52	19.04	18.56	18.68	17.80

Another possible design simplification is to locally optimize only the phasing associated with the sub-elements. Such a system would be easier to realize because implementing an adjustable phase delay is easier than implementing adjustable gain and phase delay together. Using the same scenario as before with the same local

optimization algorithm, the resulting performance is on average only 0.3 dB less then that for the locally optimized super-element system that uses complex gain for weightings and 2.2 dB less than that for the true optimal with no super-elements.

6.2 Closed Form Optimization

If the PAS is consistently changing but accurate information about the full covariance matrix is regularly available then a closed form approach might be more desirable. This would be the case if limited processing power made local optimization methods such as a gradient search prohibitive. The approaches outlined in this section require knowledge of the full covariance matrix for all array sub-elements. This can be computed directly or using the PAS

Since the optimal solution can not be solved for in closed form, alternative approaches must be adopted. The first of these approaches attempts to maximize the power received from the PAS relative to the power transmitted for each super-element individually. The second approach is an attempt to effectively span the space defined by the optimal weighting vectors.

6.2.1 Covariance Approach

The motivation for this approach is that locally optimizing the performance of each super-element should result in better performance for the array as a whole. This super-element optimization is achieved by defining the sub-element covariance matrix $\widetilde{\mathbf{C}}$ for a single super-element to be

$$\widetilde{C}_{nq} = \int \overline{\mathbf{z}}_n(\Omega) \cdot \overline{\overline{\mathbf{P}}}(\Omega) \cdot \overline{\mathbf{z}}_q^*(\Omega)\ d\Omega, \tag{6.1}$$

where $\overline{\mathbf{z}}_n(\Omega)$ represents the open circuit radiation pattern of the nth sub-element. The received power for weighting vector $\mathbf{w}$ is $\mathbf{w}^T\widetilde{\mathbf{C}}\mathbf{w}^*$. The radiated power can be fixed to γ by enforcing the constraint $\mathbf{w}^\dagger\widetilde{\mathbf{A}}\mathbf{w} = \gamma$ and

$$\widetilde{A}_{nq} = \frac{1}{2\eta_0}\int \overline{\mathbf{z}}_n^*(\Omega) \cdot \overline{\mathbf{z}}_q(\Omega)\ d\Omega. \tag{6.2}$$

Parameterizing $\mathbf{w}_m$ using $\mathbf{w} = \gamma^{1/2}\widetilde{\mathbf{A}}^{-1/2}\bar{\mathbf{w}}$ so that $\bar{\mathbf{w}}\bar{\mathbf{w}}^{\dagger} = 1$ leads to received power $\bar{\mathbf{w}}^{T}\bar{\mathbf{C}}\bar{\mathbf{w}}^{*}$ where $\bar{\mathbf{C}} = \gamma\widetilde{\mathbf{A}}^{-1/2}\widetilde{\mathbf{C}}\widetilde{\mathbf{A}}^{-1/2}$. Using an eigen-decomposition of $\bar{\mathbf{C}}$, the performance of each super-element can be optimized by choosing $\bar{\mathbf{w}}$ to be the conjugate of the eigenvector corresponding to the largest eigenvalue of $\bar{\mathbf{C}}$. The math used in this approach is identical to that used to find the optimal array. This approach does not achieve optimal results, but by optimizing each super-element locally, the performance of the entire array can be improved. When this approach is adopted for the PASs used in the computations above, the average diversity gain is only 0.6 dB less than that found using the local optimization search and 2.5 dB less than that of the true optimal.

6.2.2 Current Approach

The use of super-elements requires fixing the ratio between weights for sets of sub-elements. This leads to the idea that near optimal array performance can be achieved by choosing the sub-element weights to approximate the unrestricted weights from the optimal array. To do this, the fixed sub-element weights associated with a given super-element should approximate the weights applied to those same sub-elements for each optimal element in the unconstrained array.

Formalizing this concept requires development of some appropriate terminology. Let the mth super-element S_m be composed of sub-elements (j, k, l) with weights $\mathbf{w}_m$, and further let $\mathbf{b}_i^m$ be a vector containing weights from $\mathbf{b}_i$ for the sub-elements in super-element S_m. When weight vector $\mathbf{b}_i$ is used, the received power observed is Λ_i. Having this terminology in place, the performance metric P_m is defined for each super-element to be

$$P_m = \max \sum_{i}^{N} \Gamma_i \cos^2 \theta_i^m, \tag{6.3}$$

where θ_i^m is the angle between $\mathbf{b}_i^m$ and $\mathbf{w}_m$ and Γ_i is a scalar. The number N is a design choice corresponding to the number of optimal modes accounted for in the approximation. Experiments reveal that $N = 4$ works well. If $N = 1$, the weights are

chosen so that the dominant unconstrained antenna weights determine all sub-element weights. Γ_i is defined as

$$\Gamma_i = \Lambda_i \|\mathbf{b}_i^m\|^2, \tag{6.4}$$

The motivation for this choice is that scaling by the received power results in a better approximation of the more dominant modes. In addition, scaling by the squared norm of $\mathbf{b}_i^m$ places additional weight on sub-elements that are important to a given optimal antenna. Noting that $\cos\theta_i^m = |\mathbf{b}_i^{m\dagger}\mathbf{w}_m|/(\|\mathbf{b}_i^m\|\|\mathbf{w}_m\|)$ it is easy to see that that

$$\cos^2\theta_i^m = \frac{\mathbf{w}_m^\dagger \mathbf{b}_i^m \mathbf{b}_i^{m\dagger}\mathbf{w}_m}{\|\mathbf{b}_i^m\|^2 \mathbf{w}_m^\dagger \mathbf{w}_m}. \tag{6.5}$$

Substituting (6.5) and (6.4) into (6.3), P_m can be found by maximizing

$$P_m = \max \sum_i^N \Lambda_i \frac{\mathbf{w}^\dagger \mathbf{b}_i^m \mathbf{b}_i^{m\dagger}\mathbf{w}}{\mathbf{w}^\dagger\mathbf{w}}. \tag{6.6}$$

This maximization occurs when

$$\mathbf{w}_m = \arg\max_{\mathbf{w}} \sum_i^N \Lambda_i \frac{\mathbf{w}^\dagger \mathbf{b}_i^m \mathbf{b}_i^{m\dagger}\mathbf{w}}{\mathbf{w}^\dagger\mathbf{w}}. \tag{6.7}$$

Rearranging terms and defining $\widetilde{\mathbf{B}}_m = \sum_i^N \Lambda_i \mathbf{b}_i^m \mathbf{b}_i^{m\dagger}$, the problem can be rewritten as

$$\mathbf{w}_m = \arg\max_{\mathbf{w}} \frac{\mathbf{w}^\dagger \widetilde{\mathbf{B}}_m \mathbf{w}}{\mathbf{w}^\dagger\mathbf{w}}. \tag{6.8}$$

The solution to this optimization is when $\mathbf{w}_m$ is the eigenvector corresponding to the largest eigenvalue of $\widetilde{\mathbf{B}}_m$. Using this approach for the same configuration used in the previous examples results in the the diversity gain for the different PASs shown in Table 6.2.1. The average reduction in diversity gain is 0.8 dB relative to the locally optimized solution and 2.7 dB relative to the unconstrained optimal.

6.3 Summary

Implementing a MIMO array that achieves the optimal performance bound is difficult and costly. This chapter proposed an alternative scheme which achieves improved performance and can adapt to a PAS that changes with time. This involves combining basis functions or sub-elements into super-elements which are then combined in the same way as the optimal array. Performing the signal combining in this way facilitates significant simplifications in weighting and sampling the incoming signals. Several approaches were proposed for determining the sub-element weighting for this architecture including an iterative local optimization and two other closed form approaches.

Chapter 7

Conclusions

In this thesis, an optimality bound for MIMO antenna array performance is formulated. Because the design is based on the stochastic description of the propagation environment, the results are optimal over the ensemble of channel realizations. The optimal antenna array is found by determining the eigenfunctions of the spatial correlation operator. The solution to this problem is found as a basis function expansion of the optimal radiating currents. The performance indicated by the optimality bound is achievable if all the basis functions used in the expansion can be physically combined the same way.

The impractical nature of receiving and accurately combining a large number incoming signals makes finding a way to achieve near optimal performance with a reduced number of antennas desirable. A synthesis procedure was given for optimally placing a small number of dipoles using a genetic algorithm which resulted favorable performance. The other simplified array architecture proposed here is the super-element array. Prototyping the array configuration and then validating the weighting algorithms would be a first step in subsequent research. One of the proposed methods for determining the sub-element weighting in the super-element array was to perform a local optimization search while the array was operating. Further exploration into the validity of this approach, as well as potential algorithms for implementation would be valuable extensions to the research presented here.

The most significant contribution of the research developed here is the introduction of the optimality bound for MIMO array performance. The problems analyzed here considered a field that was vertically polarized and was restricted to the horizontal plane. This simplification was adopted for computational efficiency and

the resulting model worked well with the dipoles considered in the computational examples. The synthesis procedure achieves improved performance by simply placing the dipoles optimally. The framework developed in defining the optimal bound is not restricted to small dipole arrays. The most powerful extension of this research would be to use that fact to determine practical antenna configurations for any propagation environment. This could involve the use of other antenna architectures such as patch or slot antennas as well as experimentation with polarization diversity. Such an antenna synthesis procedure could provide a substantial improvement in performance compared to the dipole arrays proposed here.

Bibliography

[1] O. Nørklit, P. D. Teal, and R. G. Vaughan, "Measurement and evaluation of multi-antenna handsets in indoor mobile communication," *IEEE Trans. Antennas Propagat.*, vol. 49, pp. 429–437, Mar. 2001. 1, 9, 11, 15

[2] R. G. Vaughan and J. B. Andersen, "Antenna diversity in mobile communications," *IEEE Trans. Veh. Technol.*, vol. VT-36, pp. 147–172, Nov. 1987. 1, 14

[3] M. A. Jensen and J. W. Wallace, "A review of antennas and propagation for MIMO wireless communications," *IEEE Trans. Antennas Propag.*, vol. 52, pp. 2810–2824, Nov. 2004. 1, 13

[4] L. Hanlen and M. Fu, "Wireless communication systems with-spatial diversity: a volumetric model," *IEEE Trans. Commun.*, vol. 5, pp. 133–142, January 2006. 2, 13

[5] S. Nordebo, M. Gustafsson, and G. Kristensson, "On the capacity of the free space antenna channel," in *Proc. 2006 IEEE Antennas and Propag. Society Intl. Symp.*, Albuquerque, NM, Jul. 9-14 2006, pp. 3105–3108.

[6] J. W. Wallace and M. A. Jensen, "Intrinsic capacity of the MIMO wireless channel," in *Proc. 2002 IEEE Antennas and Propag. Society Intl. Symp.*, vol. 3, San Antonio, TX, Jun. 16-21 2002, pp. 198–201.

[7] M. Jensen and J. Wallace, "Antenna-independent capacity bound of electromagnetic channels," in *Proc. 2005 IEEE Antennas and Propag. Society Intl. Symp.*, vol. 2A, Washington, DC, Jul. 3-8 2005, pp. 317–320. 2, 13

[8] Y. Rahmat-Samii and E. Michielssen, *Electromagnetic Optimization by Genetic Algorithm*. John Wiley and Sons, New York, NY, 1999. 3, 41

[9] I. Telatar, "Capacity of multi-antenna gaussian channels,," *Bell Labs Tech. Memo,*, 1995. 6

[10] G. Raleigh and J. Cioffi, "Spatio-temporal coding for wireless communication," *IEEE Trans. Commun.*, vol. 46, pp. 357 – 366, March 1998. 7

[11] T. L. Marzetta and B. M. Hochwald, "Capacity of a mobile multiple-antenna communication link in Rayleigh flat fading," *IEEE Trans. Information Theory*, vol. 45, pp. 139–157, Jan. 1999. 8

[12] S. Jafar and A. Goldsmith, "Multiple-antenna capacity in correlated rayleigh fading with channel covariance information," *IEEE Antennas and Propagation Magazine.*, vol. 4, pp. 990–997, May 2005. 8

[13] L. Schumacher, K. Pedersen, and P. Mogensen, "From antenna spacings to theoretical capacities - guidelines for simulating mimo systems," in *Proc. 2002 IEEE 13th Intl. Symp. on Personal, Indoor and Mobile Radio Comm.*, vol. 2, Lisboa, Portugal, Sep. 15-18 2002, pp. 587–592. 14

[14] K. Mardia, J. Kent, and J. Bibby, *Multivariate Analysis.* Academic Press, 1980. 14

[15] J. A. Kong, *Electromagnetic Wave Theory.* John Wiley & Sons, 1990. 16

[16] N. Bikhazi and M. Jensen, "The relationship between antenna loss and superdirectivity in mimo systems," *IEEE Trans. Wireless Commun.*, vol. 6, pp. 1796–1802, May 2007. 17, 19

[17] Y. T. Lo, S. W. Lee, and Q. H. Lee, "Optimization of directivity and signal-to-noise ratio of an arbitrary antenna array," *Proc. IEEE*, vol. 54, pp. 1033–1045, Aug. 1966.

[18] S. M. Sanzgiri and J. K. Butler, "Constrained optimization of the performance indices of arbitrary array antennas," *IEEE Trans. Antennas Propag.*, vol. AP-19, pp. 493–498, Jul. 1971.

[19] M. Uzsoky and L. Solymar, "Theory of super-directive linear antennas," *Acta Physica Hungarica*, vol. 6, no. 2, pp. 185–205, 1956. 17

[20] T. K. Moon and W. C. Stirling, *Mathematical Methods and Algorithms for Signal Processing.* Prentice-Hall, 2000. 18

[21] D. H. Brandwood, "A complex gradient operator and its application in adaptive array theory," *IEE Proceedings F: Communications Radar and Signal Processing*, vol. 130, pp. 11–16, Feb. 1983. 18

[22] G. Burke and A. J. Poggio, *Numerical Electromagnetics Code (NEC)-Method of Moments*, January 1981. 26

[23] M. Morris and M. Jensen, "Network model for mimo systems with coupled antennas and noisy amplifiers," *IEEE Trans. Antennas Propag.*, vol. 53, pp. 545–552, Jan. 2005. 27

[24] K. Warnick and M. Jensen, "Effects of mutual coupling on interference mitigation with a focal plane array," *IEEE Trans. Antennas Propag.*, Aug. 2005. 27

[25] J. Johnson and V. Rahmat-Samii, "Genetic algorithms in engineering electromagnetics," *IEEE Trans. Wireless Commun.*, vol. 39, pp. 7–21, August 1997. 40